Supporting Information for

Taming Dinitramide Anions within an Energetic Cationic Metal-Organic Framework via Simple Anion Exchange: A New Strategy for Synthesis and Tunable Properties of High Energy Materials

Jichuan Zhang, Yao Du, Kai Dong, Hui Su, Shaowen Zhang, Shenghua Li* and Siping Pang*

School of Materials Science & Engineering, Beijing Institute of Technology, South Street No. 5, Zhongguancun, Haidian District, Beijing, 100081, China.

E-mail: lishenghua@bit.edu.cn; pangsp@bit.edu.cn.

Content

Caution! Although none of the complexes described herein have exploded or detonated in the course of this research, these materials should be handled with extreme care using the best safety practices.

1. **Preparation of MOF(Cu)**.

According to the previous synthetic procedure,[1] 4,4′-azo-1,2,4-triazole (atrz, 1.5 mmol, 0.246 g) in a 40 mL of boiling H_2O was added into a 20 mL [$Cu(NO_3)_2{\cdot}3H_2O$] (0.45 mmol, 0.109 g) boiling aqueous solution. The mixed solution was stirred for 1 h, and then the resulting solution was filtered. Blue crystals were obtained by slow evaporation in a glass vial within several days. Yield: 81%. Elemental analysis (%) calculated for C, 21.20; H, 1.78; N, 53.56. Found: C, 21.02; H, 1.81; N, 53.41. IR (KBr pellets, λ, cm^{-1}): 3118, 1504, 1395, 1356, 1187, 1041,886, 627.

2. **The conventional hydrothermal reactions between atrz, ADN and copper salts**

Atrz (1.5 mmol, 0.246 g) in 200 mL H_2O was added into a 10 mL aqueous solution containing various copper salts (0.45 mmol) and ADN (0.45 mmol) at room temperature, since ADN is easy to decompose at high temperature (>80 ^oC). Copper salts are $Cu(CH_3COO)_2$ and $Cu(ClO_4)_2$, respectively. The resulting solutions were under static condition at room temperature. After 10 days, the resulting solutions were still transparent without the appearance of a crystal product. It is probable that atrz has poor solubility in water at relatively low temperature, which could be disadvantageous to prepare $N(NO_2)_2^-\subset$MOF(Cu) crystals .

3. **Hygroscopic experiments of $N(NO_2)_2^-\subset$MOF(Cu) and ADN**.

The samples of $N(NO_2)_2^-\subset$MOF(Cu) after desolvated and ADN were firstly placed in vacuum at 50°C for 12 h. After being dried, 0.5 g ADN, 0.49 g $N(NO_2)_2^-\subset$MOF(Cu) (sample 1), and 0.765 g $N(NO_2)_2^-\subset$MOF(Cu) (sample 2) were then respectively placed in three vials, which were not sealed in air at room temperature. The weight of every sample was measured after every two days. The weights of these samples were shown in **Table S1.** The results showed that $N(NO_2)_2^-\subset$MOF(Cu) is almost nonhygroscopic, while ADN is severely hygroscopic.

Table S1. The weight (g) of $N(NO_2)_2^- \subset$MOF(Cu) and ADN after different days in air

Sample	0 day	2 days	4 days	6 days	8 days	One month	Gaining weight%
AND	0.500	0.506	0.512	0.534	0.620	0.642	28.4%
Sample 1	0.490	0.490	0.490	0.490	0.490	0.492	0.4%
Sample 2	0.765	0.765	0.765	0.765	0.765	0.766	0.1%

4. Preparation of the mixtures of MOF(Cu) and ADN through physical mixing

0.01 mmol ADN, 0.02 mmol ADN, and 0.04 mmol ADN were physically mixed with 0.02 mmol MOF(Cu) (0.14 g), respectively. The mole ratios of ADN/MOF(Cu) were 1:2, 1:1, and 2:1. 20 mL of hexane was then added to three different mixtures, respectively. These mixtures were ultrasonicated for 30 min to ensure intimate mixing. The hexane was allowed to evaporate in air and then the samples were placed in vacuum at 40 °C for 12 h to remove any remaining hexane and moisture. These samples were used for DSC measurements.

5. Measurement of electrostatic discharge, friction, and impact sensitivities

Impact sensitivity: the impact sensitivity was tested on a type 12 tooling according to "up and down" method (Bruceton method). A 2.5 kg weight was dropped from a set height onto a 20 mg sample placed on 150 grit garnet sandpaper. Each subsequent test was made at the next lower height if explosion occurred and at the next higher height if no explosion happened. 50 drops were made from different heights, and an explosion or non-explosion was recorded to determine the results. RDX was considered as a reference compound, the impact sensitivity of RDX is 7.4 J.

Friction sensitivity: the friction sensitivity was tested on a FSKM-10 BAM friction apparatus. RDX was also used as a reference compound, and its friction sensitivity is 110 N.

Electrostatic sensitivity: the electrostatic sensitivity was tested on a FSKM 50/20K apparatus produced by OZM Research. The sample was placed between the porcelain plate and peg. The weight of leading at least one ignition in six times was recorded.

The friction sensitivity of RDX is 0.2 J. Test conditions: 25 °C (temperature); 34% (relative humidity).

6. Measurement of contant volume energy of combustion of energetic MOFs

For the calorimetric measurements, a Parr 6200 bomb calorimeter (static jacket) with a 6510 water handling system for the combustion of energetic MOFs was used. The calorimeter was calibrated by the combustion of certified benzoic acid (about 1.0 g, pellet) in an oxygen atmosphere at a pressure of 3.05 MPa. The samples (~0.3 g each) were prepared and placed in combustion pots, which were subsequently burned in a 3.05 MPa atmosphere of pure oxygen. The experimentally determined energy of combustion was obtained as the averages of three single measurements. The experimental results for the constant volume combustion energy ($\Delta_c U$) of energetic MOFs are listed in **Table S2**.

7. Modulation of the energetic properties of MOFs through changing the molar ratio of ADN to MOF(Cu)

7.1 Synthesis of various energetic MOFs through changing the molar ratio of ADN to MOF(Cu)

To exchange more even, the crystals of MOF(Cu) were very gently broken with a spatula until the consistency for each sample was that of a powder. 0.14 g MOF(Cu) (0.2 mmol) powders were then immersed in 10 mL ADN aqueous solutions with different concentrations for 7 days at room temperature. The concentrations of ADN solutions were 0.004 mol/L, 0.01 mol/L, 0.02 mol/L, 0.04 mol/L and 0.06 mol/L, respectively. The molar ratios of ADN to MOF(Cu) were 0.2:1, 0.5:1, 1:1, 2:1, and 3:1, respectively. After decanting the solution, the resultant crystals were washed thoroughly with deionized water. The crystals were immersed in anhydrous methanol for 3 days, during which the exchanged solvent was decanted and freshly replenished three times, then dried in vacuum at 50 °C for 24 h. The corresponding exchange products after desolvated with general formula $\{Cu(atrz)_3(NO_3)_x[N(NO_2)_2]_{2-x}\}_n$ ($0 \le x \le 2$) were named **1a**, **1b**, **1c**, **1d**, and **1e**, respectively.

After anion exchange, these desolvated MOFs were used for various measurements, such as PXRD, IR, elemental analysis, sensitivity and density measurement (**Table S2**). According to the results of elemental analysis, IR spectra and

HPLC-MS, the complete exchange can be accomplished when the molar ratio of the starting materials ADN to MOF(Cu) is 3:1.

(1) **1a**: MOF(Cu) (0.2 mmol, 0.14 g); 10 mL aqueous solution of ADN (0.004 mol/L). The elemental analysis data showed that its formulation is $\{Cu(atrz)_3(NO_3)_{1.96}[N(NO_2)_2]_{0.04}\}_n$

(2) **1b**: MOF(Cu) (0.2 mmol, 0.14 g); 10 mL aqueous solution of ADN (0.01 mol/L). The elemental analysis data showed that its formulation is $\{Cu(atrz)_3(NO_3)_{1.69}[N(NO_2)_2]_{0.31}\}_n$

(3) **1c**: MOF(Cu) (0.2 mmol, 0.14 g); 10 mL aqueous solution of ADN (0.02 mol/L). The elemental analysis data showed that its formulation is $\{Cu(atrz)_3(NO_3)_{1.15}[N(NO_2)_2]_{0.85}\}_n$

(4) **1d**: MOF(Cu) (0.2 mmol, 0.14 g); 10 mL aqueous solution of ADN (0.04 mol/L). The elemental analysis data showed that its formulation is $\{Cu(atrz)_3(NO_3)_{0.32}[N(NO_2)_2]_{1.68}\}_n$

(5) **1e**: MOF(Cu) (0.2 mmol, 0.14 g); 10 mL aqueous solution of ADN (0.06 mol/L). The elemental analysis data showed that its formulation is $\{Cu(atrz)_3[N(NO_2)_2]_2\}_n$

7.2 Calculation of enthalpies of formation of various energetic MOFs

The constant-volume combustion energies ($\Delta_c U$) for the desolvated MOFs were measured by an oxygen bomb calorimeter, along with MOF(Cu) and RDX as reference materials. The enthalpy of formation ($\Delta_c H^o$) was calculated from Δ_cU and a correction for change in gas volume during combustion was included (**Scheme S1**, eq 1). The standard enthalpies of formation ($\Delta_f H°$) of these energetic MOFs, MOF(Cu) and RDX were back calculated from the heats of combustion on the basis of combustion equations (Scheme S1, eqs 2-8), Hess's Law as applied in thermochemical equations (**Shceme S2**, eqs 9-15), and known standard heats of formation for copper oxide, water and carbon dioxide [$\Delta_f H°$(CuO, s) = -156.06 kJ mol^{-1}; $\Delta_f H°$(CO_2, g) = -393.51 kJ mol^{-1}; $\Delta_f H°$(H_2O, l) = -285.83 kJ mol^{-1}].[2]

1) $\Delta cH^{\circ} = \Delta cU + \Delta nRT$
[$\Delta n = \Delta n_i$ (products, g) - Δn_j (reactants, g), Δn_i or Δn_j is the total molar amount of gases in the products or reactants

2) **1a** ($C_{12}H_{12}CuN_{26.08}O_{6.04}$, s) + 12.48 O_2 (g) ⟶ CuO (s) + 6 H_2O (l) + 12 CO_2 (g) + 13.04 N_2 (g)

3) **1b** ($C_{12}H_{12}CuN_{26.62}O_{6.31}$, s) + 12.345 O_2 (g) ⟶ CuO (s) + 6 H_2O (l) + 12 CO_2 (g) + 13.31 N_2 (g)

4) **1c** ($C_{12}H_{12}CuN_{27.70}O_{6.85}$, s) + 12.075 O_2 (g) ⟶ CuO (s) + 6 H_2O (l) + 12 CO_2 (g) + 13.85 N_2 (g)

5) **1d** ($C_{12}H_{12}CuN_{29.36}O_{7.68}$, s) + 11.66 O_2 (g) ⟶ CuO (s) + 6 H_2O (l) + 12 CO_2 (g) + 14.68 N_2 (g)

6) **1e** ($C_{12}H_{12}CuN_{30}O_8$, s) + 11.5 O_2 (g) ⟶ CuO (s) + 6 H_2O (l) + 12 CO_2 (g) + 15 N_2 (g)

7) **MOF(Cu)** ($C_{12}H_{12}CuN_{26}O_6$, s) + 12.5 O_2 (g) ⟶ CuO (s) + 6 H_2O (l) + 12 CO_2 (g) + 13 N_2 (g)

8) RDX ($C_3H_6N_6O_6$, s) + 1.5 O_2 (g) ⟶ 3 H_2O (l) + 3 CO_2 (g) + 3 N_2 (g)

Scheme S1. Combustion reaction of various energetic MOFs and RDX

9) $\Delta_f H^{\circ}$ (**1a**, s} = $\Delta_f H^{\circ}$ (CuO, s) + 6 $\Delta_f H^{\circ}$ (H_2O, l) + 12 $\Delta_f H^{\circ}$ (CO_2, g) - ΔcH° (**1a**, s}

10) $\Delta_f H^{\circ}$ (**1b**, s} = $\Delta_f H^{\circ}$ (CuO, s) + 6 $\Delta_f H^{\circ}$ (H_2O, l) + 12 $\Delta_f H^{\circ}$ (CO_2, g) - ΔcH° (**1b**, s}

11) $\Delta_f H^{\circ}$ (**1c**, s} = $\Delta_f H^{\circ}$ (CuO, s) + 6 $\Delta_f H^{\circ}$ (H_2O, l) + 12 $\Delta_f H^{\circ}$ (CO_2, g) - ΔcH° (**1c**, s}

12) $\Delta_f H^{\circ}$ (**1d**, s} = $\Delta_f H^{\circ}$ (CuO, s) + 6 $\Delta_f H^{\circ}$ (H_2O, l) + 12 $\Delta_f H^{\circ}$ (CO_2, g) - ΔcH° (**1d**, s}

13) $\Delta_f H^{\circ}$ (**1e**, s} = $\Delta_f H^{\circ}$ (CuO, s) + 6 $\Delta_f H^{\circ}$ (H_2O, l) + 12 $\Delta_f H^{\circ}$ (CO_2, g) - ΔcH° (**1e**, s}

14) $\Delta_f H^{\circ}$ {MOF(Cu), s} = $\Delta_f H^{\circ}$ (CuO, s) + 6 $\Delta_f H^{\circ}$ (H_2O, l) + 12 $\Delta_f H^{\circ}$ (CO_2, g) - ΔcH° { MOF(Cu), s}

15) $\Delta_f H^{\circ}$ (RDX, s) = 3 $\Delta_f H^{\circ}$ (H_2O, l) + 3 $\Delta_f H^{\circ}$ (CO_2, g) - ΔcH° (RDX, s)

Scheme S2. Hess's Law for the combustion reaction of various energetic MOFs and RDX

7.3 Calculation of detonation properties of various energetic MOFs

We adopted two different methods for the calculation of detonation properties of various desolvated MOFs with general formula $\{Cu(atrz)_3(NO_3)_x[N(NO_2)_2]_{2-x}\}_n$. These methods are shown as follows: (i) our recently developed method on the basis of the empirical Kamlet formula[3,4]; ii) the commercial program EXPLO5 v6.01.

(i) Adopting our developed method for the calculation of detonation properties of various energetic MOFs

According to the largest exothermic principle proposed by Kamlet, the corresponding products generated from explosives containing CHON elements during detonation can be assumed in the following two equilibriums (**Scheme S3**):

16) $2CO \rightleftharpoons CO_2 + C$ $\quad \Delta H^{\circ} = -41.2$ kcal/mol

17) $H_2 + CO \rightleftharpoons H_2O + C$ $\quad \Delta H^{\circ} = -31.4$ kcal/mol

Scheme S3. Two equilibriums considered in the H_2O-CO_2 arbitrary theory

As mentioned by Kamlet, for practical calculational purposes, equilibrium 17 may be considered as invariantly to the right at all loading densities under consideration. Reaction 16, on the other hand, is in a region of shifting equilibrium and may be considered as predominantly to the right only at the higher loading densities (i.e., greater than 1.6 or 1.7 $g \cdot cm^{-3}$). In practice, an H atom should have higher priority than a C atom, because 1 mol of H_2O has a lower heat of formation than 0.5 mol of CO_2 when 1 mol of O atom is consumed; furthermore, the N value in the K-J equation should also increase. Typically, when the K-J equation is employed for calculation, the overall process can be described as follows: for the explosives composed of C, H, N, and O elements, all N atoms are converted to N_2; O atoms form H_2O with H atoms first and then form CO_2 with C atoms; the remaining C atoms are retained in solid state; if there are O atoms left, they will form O_2.

In our method, to preserve Kamlet's method, the H_2O–CO_2 arbitrary theory is employed to determine the detonation products from metal-containing explosives (CHONM). In most cases, metal atoms are converted to their oxidation states, emitting more heat after detonation. Otherwise, metal atoms can be treated as their reduction state, if the heat of formation of metallic oxides is higher than that of H_2O, or there is no O atom in the molecule. Besides, O atoms form H_2O with H atoms first and the remaining ones form CO_2 with C atoms. However, if the amount of O atoms is not sufficient to oxidize all H atoms, the remaining H atoms can produce NH_3 with N atoms, and the rest of the N atoms are released as N_2 gas. On the other hand, the remaining C atoms are retained in the solid state if they are not completely oxidized by O atoms. If there are redundant O atoms, however, they can be expelled as O_2. In addition, metallic oxides are treated as inert solids, thus no gas is produced, only heat emits in the explosion process.

According to the H_2O–CO_2 arbitrary theory, copper atoms should be converted to their reduction state (Cu) during detonation from our as-synthesized energetic MOFs since the heat of formation of copper oxide [$\Delta_f H°$(CuO, s) = -156.06 kJ mol^{-1}] is higher than that of water [$\Delta_f H°$(H_2O, g) = -241.83 kJ mol^{-1}].[2] In other words, if 1 mol of O atoms is consumed, much more heat could be released when O atoms react with H atoms rather than copper atoms. According to the above theories, the detonation reactions of our as-synthesized energetic MOFs were proposed in **Scheme S4**.

Based on the detonation reactions of energetic MOFs, their detonation properties were evaluated by the empirical Kamlet formula,[3] as follows:

$V_D = 1.01(NM^{1/2}Q^{1/2})^{1/2}(1+1.30\rho)$

$P = 1.55\ NM^{1/2}Q^{1/2}\rho^2$

$Q = -[\Delta_f H(\text{detonation products}) - \Delta_f H(\text{explosive})]/\text{formula weight of explosive}$

In the Kamlet equations, V_D represents detonation velocity (km s^{-1}) and P is detonation pressure (GPa), ρ is the density of explosive (from gas pycnometer, g cm^{-3}). Φ, N, M and Q are characteristic parameters of an explosive. N is the moles of detonation gases per gram of explosive, M is the average molecular weight of these gases and Q is the heat of detonation (kcal kg^{-1}). $\Delta_f H$(explosive) is the experiment determined (back-calculated from $-\Delta_c U$) enthalpy of formation of energetic MOF.

18) **1a** ($C_{12}H_{12}CuN_{26.08}O_{6.04}$, s) ⟶ Cu (s) + 6 H_2O (g) + 0.02 CO_2 (g) + 13.04 N_2 (g) + 11.98 C (s)

19) **1b** ($C_{12}H_{12}CuN_{26.62}O_{6.31}$, s) ⟶ Cu (s) + 6 H_2O (g) + 0.155 CO_2 (g) + 13.31 N_2 (g) + 11.845 C (s)

20) **1c** ($C_{12}H_{12}CuN_{27.70}O_{6.85}$, s) ⟶ Cu (s) + 6 H_2O (g) + 0.425 CO_2 (g) + 13.85 N_2 (g) + 11.575 C (s)

21) **1d** ($C_{12}H_{12}CuN_{29.36}O_{7.68}$, s) ⟶ Cu (s) + 6 H_2O (g) + 0.84 CO_2 (g) + 14.68 N_2 (g) + 11.16 C (s)

22) **1e** ($C_{12}H_{12}CuN_{30}O_8$, s) ⟶ Cu (s) + 6 H_2O (g) + CO_2 (g) + 15 N_2 (g) + 11 C (s)

24) MOF(Cu) ($C_{12}H_{12}CuN_{26}O_6$, s) ⟶ Cu (s) + 6 H_2O (g) + 13 N_2 (g) + 12 C (s)

25) RDX ($C_3H_6N_6O_6$, s) ⟶ 3 H_2O (g) + 1.5 CO_2 (g) + 3 N_2 (g) + 1.5 C (s)

Scheme S4. Detonation reactions of energetic MOFs and RDX

(ii) Adopting EXPLO5 v6.01 for the calculation of detonation properties of various energetic MOFs

To confirm the prediction accuracy of our developed method, we also employed EXPLO5 v6.01 to calculate the detonation properties of these MOFs. Using the molecular formula, density (from gas pycnometer), and experiment determined (back-calculated from $-\Delta_c U$) enthalpy of formation ($\Delta_f H^o$), we can use the EXPLO5 computer code in its new version 6.01 to calculate the detonation velocity (V_D), detonation pressure (P), volume of gases after detonation (Vo) and heat of detonation (Q), as illustrated in Table S2.

In summay, from Table S2, we can find that as the mole ratio of ADN/MOF(Cu) in the reaction mixture gradually increased from 0 to 3, the resultant complex also showed a gradual increase in the encapsulated quantity of $N(NO_2)_2^-$ anions, and density from 1.64 to 1.78 g cm^{-3}, detonation velocity from 6780 to 8227 m s^{-1}, detonation

pressure from 19.15 to 29.67 Gpa, volume of gases after detonation from 626 to 642 L kg^{-1}, and heat of detonation from 4562 to 7176 kJ kg^{-1} while the impact sensitivity showed a gradual decrease from 16 to 9 J. Therefore, in comparison with the previous methods for tuning the properties of energetic materials with complicated chemical modifications, this way is more simple and convenient.

8. Procedures for the controllable release of $N(NO_2)_2^-$ from $N(NO_2)_2^-$ ⊂MOF(Cu)

To exchange more even, the crystals of $N(NO_2)_2^-$⊂MOF(Cu) were very gently broken with a spatula until the consistency for each sample was that of a loose powder. $N(NO_2)_2^-$⊂MOF(Cu) powders (0.16 g, 0.2 mmol) were then immersed in 10 mL NaN_3 aqueous solutions with different concentrations for 30 min at room temperature. The concentrations of NaN_3 solutions were 0.004 mol/L, 0.01 mol/L, 0.02 mol/L, 0.04 mol/L and 0.06 mol/L, and the molar ratios of NaN_3 to $N(NO_2)_2^-$⊂MOF(Cu) were 0.2:1, 0.5:1, 1:1, 2:1, and 3:1, respectively. After decanting the solution, the resultant crystals were washed thoroughly with deionized water. The crystals were immersed in anhydrous methanol for 3 days, during which the exchanged solvent was decanted and freshly replenished three times, then dried in vacuum at 50 °C for 24 h. The corresponding solid products after desolvated were named **2a**, **2b**, **2c**, **2d**, and **2e**, respectively.

2a: $N(NO_2)_2^-$⊂MOF(Cu) (0.2 mmol, 0.16 g), 10 mL aqueous solution of NaN_3 (0.004 mol/L). The elemental analysis data showed that its formulation is $\{Cu(atrz)_3[N(NO_2)_2]_{1.80}(N_3)_{0.2}\}_n$.

2b: $N(NO_2)_2^-$⊂MOF(Cu) (0.2 mmol, 0.16 g); 10 mL aqueous solution of NaN_3 (0.01 mol/L). The elemental analysis data showed that its formulation is $\{Cu(atrz)_3[N(NO_2)_2]_{1.53}(N_3)_{0.47}\}_n$

2c: $N(NO_2)_2^-$⊂MOF(Cu) (0.2 mmol, 0.16 g); 10 mL aqueous solution of NaN_3 (0.02 mol/L). The elemental analysis data showed that its formulation is $\{Cu(atrz)_3[N(NO_2)_2](N_3)\}_n$.

2d: $N(NO_2)_2^-$⊂MOF(Cu) (0.2 mmol, 0.16 g); 10 mL aqueous solution of NaN_3 (0.04 mol/L). The elemental analysis data showed that its formulation is $\{Cu(atrz)_3[N(NO_2)_2]_{0.02}(N_3)_{1.98}\}_n$.

2e: $N(NO_2)_2^- \subset$MOF(Cu) (0.2 mmol, 0.16 g); 10 mL aqueous solution of NaN_3 (0.06 mol/L). The elemental analysis data showed that its formulation is $\{Cu(atrz)_3(N_3)_2\}_n$.

After anion release, the released $N(NO_2)_2^-$ from $N(NO_2)_2^- \subset$MOF(Cu) into aqueous solution was determined by HPLC-MS, and the concomitant solid product after desolvated was used for various measurements, such as IR, elemental analysis and sensitivity (**Table S3**). However, most of PXRD patterns and densities of solid products have not been determined since these solid products are highly sensitive to impact. The results of elemental analysis and IR spectra showed as the molar ratio of NaN_3 to $N(NO_2)_2^- \subset$MOF(Cu) increases, the encapsulated quantity of N_3^- in the resultant complex increases while the encapsulated quantity of $N(NO_2)_2^-$ decreases. It confirmed that the encapsulated $N(NO_2)_2^-$ can be controllably released through tuning the mole ratio of NaN_3 to $N(NO_2)_2^- \subset$MOF(Cu) in the reaction mixture. In addition, as the molar ratio of NaN_3 to $N(NO_2)_2^- \subset$MOF(Cu) increases from 0 to 3, the nitrogen content of the resultant complex increases from 54.81% to 64.91% while its impact sensitivity decreases 9 to 1.5 J, which indicated that the solid product can be tuned from a potential secondary explosive to a high-sensitivity primary explosive. It further confirmed that this way is more simple and convenient for tuning the properties of energetic materials.

Table S2. Element contents and energetic properties of different products after anion exchange between ADN and MOF(Cu) at different mole ratios.

Comp.	N%[a]	C%[b]	H%[c]	O%[d]	p[e]	IS[f]	ESD[g]	$-\Delta_c U$[h]	$-\Delta_f H$[i]	$\Delta_f H^o$[j]	P[k]	V_D[l]	V_o[m]	Q[n]
MOF(Cu)	53.35	21.07	1.78	14.24	1.64	16	24.75	8275.4	8244	1651	19.15[r] (18.56[s])	6780[r] (6860[s])	626[r] (698[s])	4562[r] (4388[s])
1a	53.42	21.12	1.78	14.17	1.66	12.5	21.44	8331	8300	1706	19.77[r] (20.0[s])	6863[r] (7064[s])	627[r] (697[s])	4628[r] (4471[s])
1b	53.69	20.58	1.76	14.58	1.70	12.0	18.41	8518	8468	1893	21.58[r] (21.13[s])	7117[r] (7326[s])	629[r] (700[s])	4909[r] (4728[s])
1c	54.11	20.01	1.60	15.31	1.72	11.5	9.83	9043	9009	2416	23.97[r] (24.11[s])	7473[r] (7674[s])	633[r] (708[s])	5623[r] (5385[s])
1d	54.63	19.01	1.58	16.21	1.76	9.4	4.65	9896	9859	3266	27.83[r] (28.69[s])	7995[r] (8200[s])	639[r] (719[s])	6695[r] (6374[s])
1e	54.81	18.69	1.57	16.72	1.78	9.0	2.21	10299	10261	3667	29.67[r] (30.97[s])	8227[r] (8427[s])	642[r] (723[s])	7176[r] (6824[s])
RDX[o]	37.84	16.22	2.72	43.22	1.81	7.5	0.2	2103	2092	53.83	34.37[r] (35.17[s])	8810[r] (8810[s])	756[r] (791[s])	6168[6] (5668[s])
RDX[p]	37.84	16.22	2.72	43.22	1.81	7.5	0.2	-	-	70.3	34.5[s]	8861[s]	785[s]	5845[s]
Cl-20[q]	38.36	16.45	1.38	43.81	2.04	4	0.13	-	-	365	44.4[s]	9730[s]	715[s]	6168[s]

[a]Determined nitrogen content. [b]Determined carbon content. [c]Determined hydrogen content. [d]Determined oxygen content. [e]Density measured by gas pycnometer (g cm^{-3}, 25 ℃). [f]Impact sensitivity (J). [g]Electrostatic sensitivity (J). [h]Experimental determined (oxygen bomb calorimetry) contant volume energy of combustion (kJ mol^{-1}). [i]Expremental molar enthalpy of combustion (kJ mol^{-1}) [j]Experiment determined (back-calculated from $-\Delta_c U$) enthalpy of formation (kJ mol^{-}). [k]Detonation pressure (GPa). [l]Detonation velocity (m s^{-1}). [m]Volume of gases after detonation (L kg^{-1}). [n]Heat of detonation (kJ kg^{-1}). [o]Detonation properties of RDX (as a reference compound) were obtained on the basis of its experiment determined (back-calculated from $-\Delta_c U$) enthalpy of formation. [p]Properties of RDX are taken from ref 5. [q]Properties of CL-20 are taken from ref 6. [r]The detonation properties were calculated by our developed method. [s]The detonation properties were calculated by EXPLO5 v6.01.

MOF(Cu): $[Cu(atrz)_3(NO_3)_2]_n$, $CuC_{12}H_{12}N_{26}O_6$, M=680; **1a**: $\{Cu(atrz)_3(NO_3)_{1.96}[N(NO_2)_2]_{0.04}\}_n$, $CuC_{12}H_{12}N_{26.08}O_{6.04}$, M=683.8; **1b**: $\{Cu(atrz)_3(NO_3)_{1.69}[N(NO_2)_2]_{0.31}\}_n$, $CuC_{12}H_{12}N_{26.62}O_{6.31}$, M=693.6; **1c**: $\{Cu(atr)_3(NO_3)_{1.15}[N(NO_2)_2]_{0.85}\}_n$, $CuC_{12}H_{12}N_{27.7}O_{6.85}$, M=717.4; **1d**: $\{Cu(atr)_3(NO_3)_{0.32}[N(NO_2)_2]_{1.68}\}_n$, $CuC_{12}H_{12}N_{29.36}O_{7.68}$, M=753.9; **1e**: $[N(NO_2)_2^- \subset MOF(Cu)]$: $\{Cu(atr)_3[N(NO_2)_2]_2\}_n$, $C_{12}H_{12}CuN_{30}O_8$, M=768.

Table S3. Element contents and sensitivities of different products after anion release between $N(NO_2)_2^- \subset$MOF(Cu) and NaN_3 at different mole ratios.

Comp.	N%[a]	C%[b]	H%[c]	O%[d]	IS[e]	Formulation
$N(NO_2)_2^- \subset$MOF(Cu)	54.81	18.69	1.57	16.72	9	$\{Cu(atrz)_3[N(NO_2)_2]_2\}_n$
2a	55.40	18.91	1.70	15.23	7.5	$\{Cu(atrz)_3[N(NO_2)_2]_{1.80}(N_3)_{0.2}\}_n$
2b	56.82	19.32	1.74	13.40	3.5	$\{Cu(atrz)_3[N(NO_2)_2]_{1.53}(N_3)_{0.47}\}_n$
2c	59.42	20.21	1.81	9.28	3	$\{Cu(atrz_3[N(NO_2)_2]\ (N_3)\}_n$
2d	64.82	22.33	1.85	<0.03	1.5	$\{Cu(atrz)_3[N(NO_2)_2]_{0.02}(N_3)_{1.98}\}_n$
2e	64.91	22.41	1.86	<0.03	1.5	$\{Cu(atrz)_3(N_3)_2\}_n$

[a]Determined nitrogen content. [b]Determined carbon content. [c]Determined hydrogen content. [d]Determined oxygen content. [e]Impact sensitivity (J).

$N(NO_2)_2^- \subset$ MOF(Cu): $\{Cu(atr)_3[N(NO_2)_2]_2\}_n$, $CuC_{12}H_{12}N_{30}O_8$, M= 768; **2a**: $\{Cu(atrz)_3[N(NO_2)_2]_{1.8}(N_3)_{0.2}\}_n$, $CuC_{12}H_{12}N_{30}O_{7.2}$, M=755.2; **2b**: $\{Cu(atrz)_3[N(NO_2)_2]_{1.53}(N_3)_{0.47}\}_n$, $CuC_{12}H_{12}N_{30}O_{6.12}$, M=737.9; **2c**: $\{Cu(atrz)_3[N(NO_2)_2](N_3)\}_n$, $CuC_{12}H_{12}N_{30}O_4$, M=704; **2d**: $\{Cu(atrz)_3[N(NO_2)_2]_{0.02}(N_3)_{1.98}\}_n$, $CuC_{12}H_{12}N_{30}O_{0.08}$, M=641.3 ; **2e**: $\{Cu(atrz)_3(N_3)_2\}_n$, $CuC_{12}H_{12}N_{30}$, M=640.

Table S4. Comparison of density, oxygen and nitrogen content of some reported energetic MOFs with desolvated $N(NO_2)_2^- \subset MOF(Cu)$

Comp.	ρ[a]	O%[b]	(N+O)%[c]	Ref.
$N(NO_2)_2^- \subset$ MOF(Cu)	1.78	16.72	**71.53**	This work
MOF(Cu)	1.68	14.12	67.65	*Angew. Chem. Int. Ed.* **2013**, 52, 14031-14035
MOF(Ag)	2.16	11.54	55.29	*Angew. Chem. Int. Ed.* **2013**, 52, 14031-14035
CHP	1.948	30.62	64.11	*J. Am. Chem. Soc.* **2012**, *134*, 1422-1425
NHP	1.983	30.64	64.16	*J. Am. Chem. Soc.* **2012**, *134*, 1422-1425
CHHP	2.0	33.93	56.76	*Chem. Eur. J.* **2013**, *19*, 1706-1711
ZnHHP	2.117	35.02	58.59	*Chem. Eur. J.* **2013**, *19*, 1706-1711
MOF(Co)	1.707	6.34	66.22	*Chem. Eur. J.* **2014**, *20*, 1 – 6
MOF(Pb1)	2.519	3.22	42.62	*J. Mater. Chem. A*, **2014**, *2*, 11958–11965
MOF(Pb2)	3.511	4.44	31.64	*J. Mater. Chem.A*, **2014**, *2*, 11958–11965
MOF(Cu1)	1.885	8.61	61.32	*Green Chem.*, **2015**, *17*, 831–836
MOF(Cu2)	2.308	7.39	52.62	*Green Chem.*, **2015**, *17*, 831–836
MOF(Cu3)	2.419	0	49.08	*Green Chem.*, **2015**, *17*, 831–836
MOF(CuNa)	1.975	0	40.08	*Dalton Trans.*, **2015**, *44*, 2333-2339
MOF(K2)	2.09	39.8	66.7	*RSC Adv.* **2015**, DOI: 10.1039/C5RA09822J
MOF(Ag2)	2.966	0	29.32	*New. J. Chem.* **2015**, DOI: 10.1039/C5NJ01623A
MOF(Ag3)	3.121	14.48	38.82	*New. J. Chem.* **2015**, DOI: 10.1039/C5NJ01623A
MOF(CuN_3)	2.03	30.28	52.37	*RSC Adv.* **2014**, *4*, 16087-16093

[a]Density from X-ray diffration analysis (g cm^{-3}). [b]Oxygen content. [c]Nitrogen and oxygen content.

$N(NO_2)_2^- \subset$ MOF(Cu): $[\{Cu(C_4H_4N_8)_3[N(NO_2)_2]_2\}]_n$, $C_{12}H_{12}CuN_{30}O_8$, M=768; **MOF(Cu):** $\{Cu(C_4H_4N_8)_3(NO_3)_2\}_n$, $CuC_{12}H_{12}N_{26}O_6$, M=680; **MOF(Ag):** $[Ag(C_4H_4N_8)_{1.5}NO_3]_n$, $AgC_6H_6N_{13}O_3$, M=416; **CHP**: $[Co(N_2H_4)_5(ClO_4)_2]_n$, $CoN_{10}H_{20}O_8Cl_2$, M=418; **NHP:** $[Ni(N_2H_4)_5(ClO_4)_2]_n$, $NiN_{10}H_{20}O_8Cl_2$, M=417.7; **CHHP:** $[Co_2(N_2H_4)_4(N_2H_3CO_2)_2(ClO_4)_2]\cdot H_2O]_n$, $Co_2C_2H_{24}N_{12}O_{13}Cl_2$, M=613.09; **ZnHHP:** $\{[Zn_2(N_2H_4)_3(N_2H_3CO_2)_2(ClO_4)_2]\cdot H_2O\}_n$, $Zn_2C_2H_{20}N_{10}O_{13}Cl_2$, M=593.92; **MOF(Co)**: $[Co_9(C_2HN_9)_{10}(C_2H_2N_9)_2(H_2O)_{10}]_n$, $Co_9C_{24}H_{34}N_{108}O_{10}$, M=2525; **MOF(Pb1):** $[Pb(C_3H_3N_7)_2(H_2O)]_n$, $PbC_6H_6N_{14}O$, M=497.45; **MOF(Pb2)**: $[Pb(C_3H_3N_7)(O)]_n$, $PbC_3H_3N_7O$, M=360.31; **MOF(Cu1):** $[Cu(C_3H_2N_7)_2(H_2O)_2]_n$, $CuC_6H_8N_{14}O_2$, M=371.8; **MOF(Cu2):** $[Cu(C_3HN_7)\cdot H_2O]_n$, $CuC_3H_3N_7O$, M=216.65; **MOF(Cu3):** $[Cu(C_3H_2N_7)]_n$, $CuC_3H_2N_7$, M=199.66; **MOF(CuNa)**: $[Cu_4Na(CH_4N_4)_5(CH_3CN)]_n$, $Cu_4NaN_{21}C_{12}H_{18}$, M=735; **MOF(K2)**: $[C_8K_2N_{10}O_{13}]_n$, M=522.4; **MOF(Ag2)**: $[AgC_2H_3N_4]_n$, M=191.0; **MOF(Ag3)**: $[AgC_2H_2N_4O_2]_n$, M=221.0; **MOF(CuN_3)**: $[C_7H_3CuN_5O_6]_n$, M=317.

Table S5. Crystallographic data and strucutre refinement parameters for $N(NO_2)_2^-$ ⊂MOF(Cu) and MOF(Cu)

	MOF (Cu)	**$N(NO_2)_2^-$ ⊂ MOF(Cu)**
CCDC	955533	1057051
Empirical formula	$C_{12}H_{12}CuN_{26}O_6$	$C_{12}H_{12.92}CuN_{30}O_{8.46}$
Formula mass	679.94	776.34
Crystal system	monoclinic	monoclinic
Space group	P 2(1)/n	P 2(1)/n
Z	2	2
a (Å)	8.0107(17)	8.1156(6)
b (Å)	20.461(5)	20.3861(11)
c (Å)	8.6435(19)	8.6579(4)
α (°)	90	90
β (°)	90.643(2)	91.199(6)
γ (°)	90	90
Volume ($Å^3$)	1416.6(6)	1432.10(15)
D_{calc} (g cm^{-3})	1.68	1.801
Temperature (K)	153	99
F(000)	726.0	783.2
h, k, l	10,28,11	10, 26, 11
μ (cm-1)	0.816	0.864
R_1 [I > 2σ(I)]	0.0449	0.0606
Reflections collected	11511	2101
Completeness to theta full (%)	0.977	0.993
wR_2 (all data)	0.1235	0.1538
S on *F2*	1.000	1.076

As shown in Table S5, most of crystallographic data and structure refinement parameters for $N(NO_2)_2^-$ ⊂MOF(Cu) crystals are almost consistent with those of MOF(Cu), such as crystal system, space group, Z, a, b, c, α, β, and γ. These results show that the framework remained intact throughout the exchange process.

Table S6. Selected bond lengths (Å) and bond angles (°) in crystals for $N(NO_2)_2^-$ ⊂MOF(Cu) and MOF (Cu)

Bond	MOF (Cu)	$N(NO_2)_2^-$ ⊂ MOF(Cu)
N1-N2	1.401(2)	1.394(8)
N2-C2	1.301(3)	1.302(9)
N3-C1	1.353(3)	1.355(9)
N4-N4′	1.227(2)	1.241(9)
N1-C1	1.296(3)	1.294(9)
C2-N3	1.373(3)	1.381(9)
N3-N4	1.390(3)	1.405(8)
C1-H1	0.951(2)	0.950(2)
Cu1-Cu7	11.822(2)	11.825(2)
N8-O1	1.233(6)	1.295(28)
N8-O2	1.238(5)	1.269(23)
N8-N9		1.343(23)
N9-N10		1.373(17)
N10-O3		1.333(13)
N10-O4		1.214(16)
Bond angels	**MOF(Cu)**	**$N(NO_2)_2^-$ ⊂ MOF(Cu)**
N7-Cu1-N1′	180.000(65)	180.000
N6-Cu1-N8	90.937(65)	90.7(2)
N7-Cu1-N6	92.049(63)	91.1(2)
Cu1-N1′-C1′	122.495(151)	122.0(5)
N1′-Cu-N6	87.971(63)	88.9(2)
N7-Cu1-N8	90.044(60)	90.1(2)
N5-Cu1-N6	180.000	180.000
Cu1-N1’-N2′	126.853(119)	126.1(4)
N1′-Cu1-N8	89.651(60)	89.9(2)
N7-Cu1-N8	90.937(65)	90.1(2)
N8-Cu1-N9	180.000(65)	180.0(4)
C1′-N1′-N2′	108.136(172)	107.7(6)
N1′-Cu1-N8	89.651(60)	89.9(2)
N7-Cu1-N8	90.937(65)	90.1(2)
N8-Cu1-N9	180.000(65)	180.0(4)
C1′-N1′-N2′	108.136(172)	107.7(6)
O1-N8-O2	114.488(323)	122.847(1703)
O1-N8-N9		120.280(1806)
N8-N9-N10		108.698(1149)
N9-N10-O4		123.137(1153)

Table S7. Selected bond lengths (N8-N9 and N9-N10) and bond angles (N8-N9-N10) of $N(NO_2)_2^- \subset$ MOF(Cu) and other compounds containing dinitramide ion

	N8-N9	N9-N10	N8-N9-N10
$N(NO_2)_2^- \subset$ MOF(Cu)	1.343(23)	1.373(17)	108.698(115)
$NH_4N(NO_2)_2$[7]	1.376(1)	1.359(1)	113.2(8)
$KN(NO_2)_2$[7]	1.384(3)	1.351(3)	114.0(2)
$CsN(NO_2)_2$[7]	1.377(8)	1.360(8)	115.1(4)
$LiN(NO_2)_2$[8]	1.366(3)	1.366(3)	114.5(2)
$[Ag(py)_2][N(NO_2)_2]$[9]	1.345(7)	1.360(7)	112.2(5)
$[Cu(NH_3)_4][N(NO_2)_2)]_2$[9]	1.364(3)	1.386(3)	113.9(2)
$C_4H_{10}N_{10}[N(NO_2)_2]_2$[10]	1.349(2)	1.391(1)	115.4(1)
$CH_5N_6[N(NO_2)_2]$[11]	1.355(2)	1.377(2)	116.0(2)
$CH_5N_6[N(NO_2)_2]$[11]	1.353(3)	1.393(3)	115.4(2)
$CH_4N_5[N(NO_2)_2]$[12]	1.375(2)	1.372(2)	116.0(1)
$CH_4N_5[N(NO_2)_2]$[12]	1.352(2)	1.384(2)	114.7(1)
$CH_3N_4[N(NO_2)_2]$[12]	1.336(3)	1.336(3)	115.8(2)

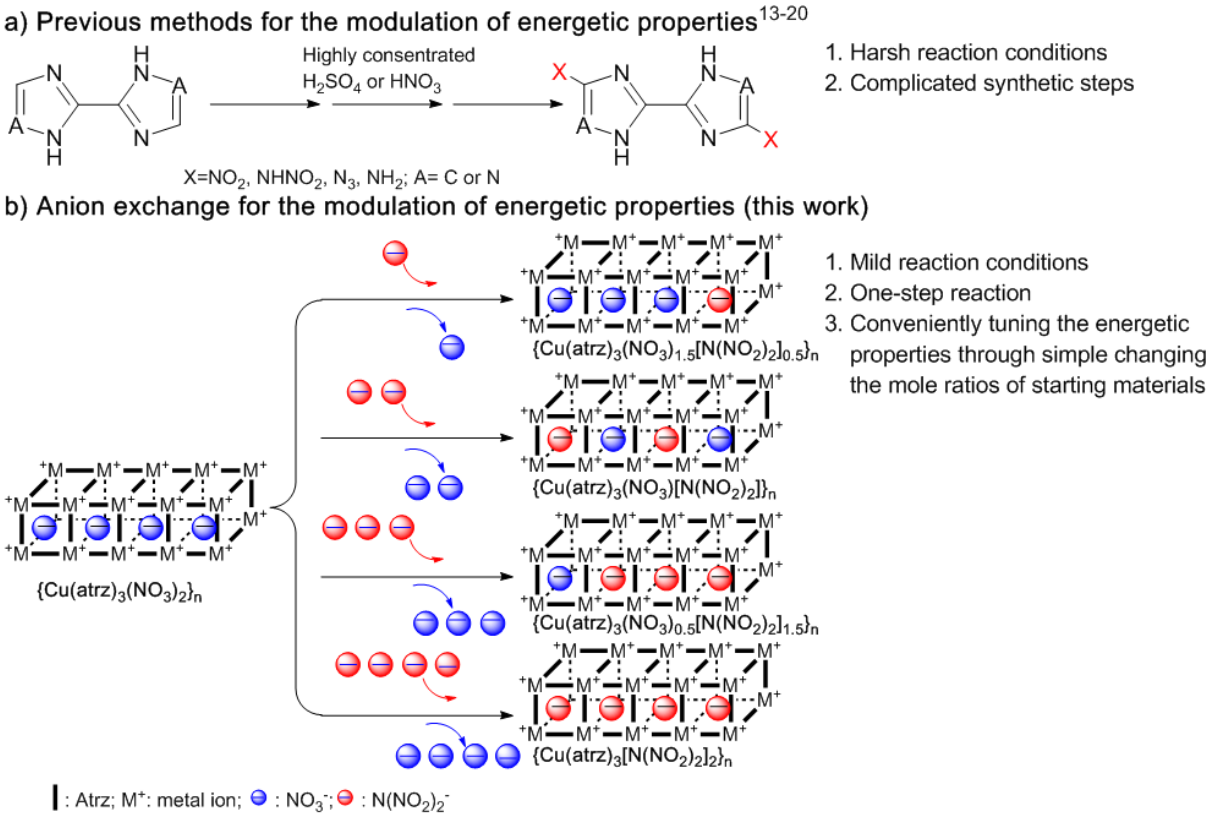

Figure S1. Various strategies for the modulation of energetic properties.

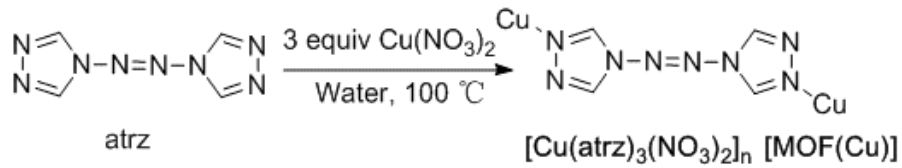

Figure S2. Synthesis, coordination mode, and formulae for MOF(Cu)

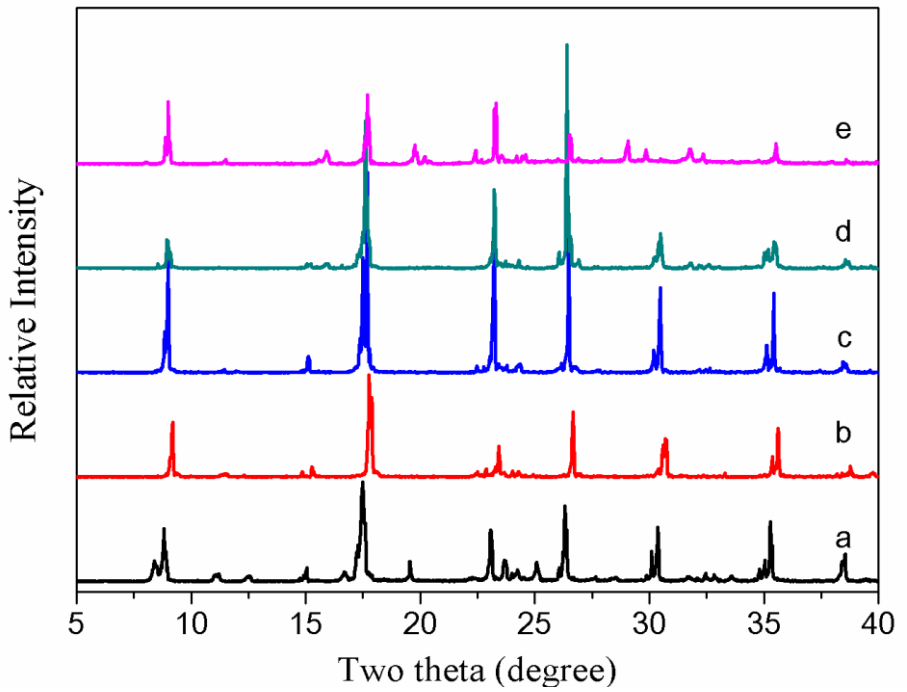

Figure S3. PXRD patterns of as-prepared MOF(Cu) in various HNO_3/NaOH aqueous solutions with different pH values for 24 hours: a) pH=1; b) pH=4; c) pH=7; d) pH=10; e) pH=14. The PXRD patterns showed that MOF(Cu) can keep its crystallinity after immersion in HCl/NaOH aqueous solutions with pH values ranging from 0 to 10 for 24 h.

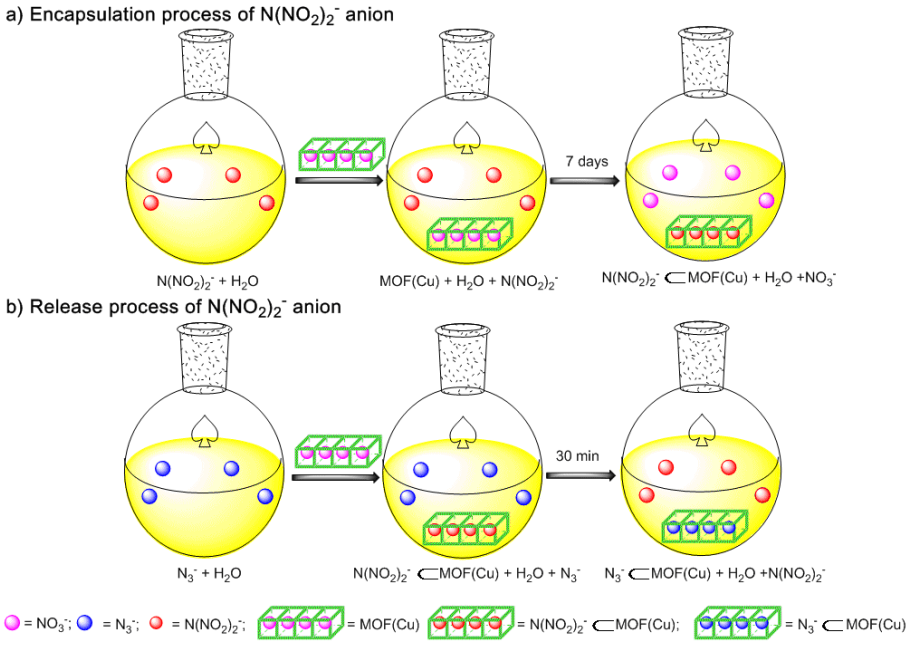

Figure S4. Encapsulation and release process of $N(NO_2)^-$ anion

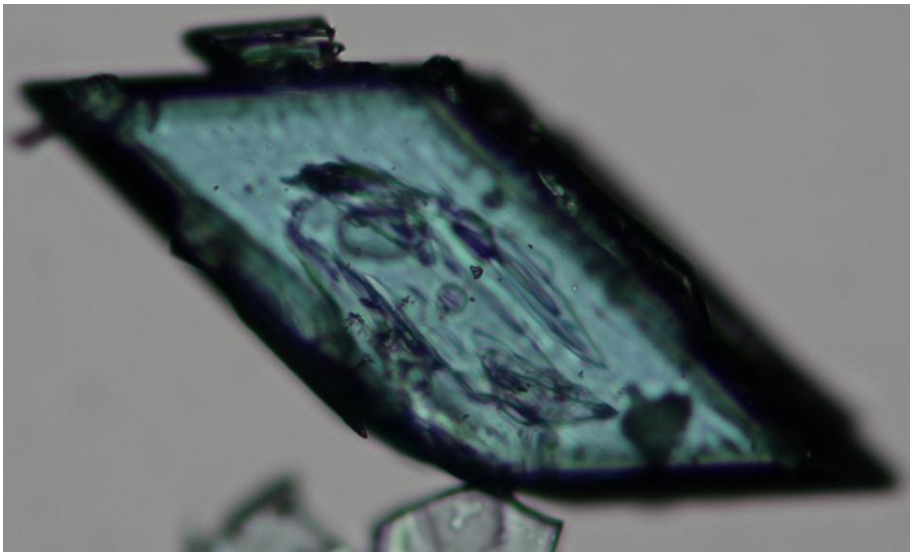

Figure S5. Photograph of $N(NO_2)_2^-$⊂MOF(Cu) crystals

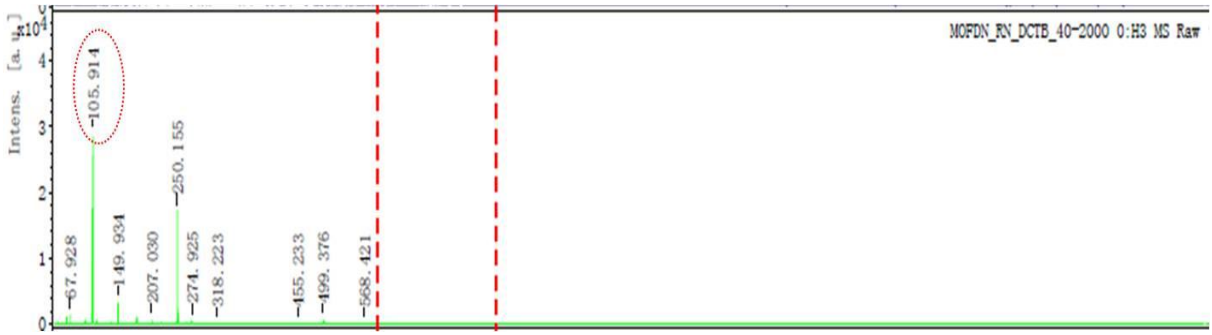

Figure S6. MOLDI-TOF-MS spectrum of $N(NO_2)_2^-$⊂MOF(Cu) crystals. MOLDI-TOF negative ion mode: the mass-charge ratio of $[N(NO_2)_2]^-$ is m/z 105.91.

The result showed that $N(NO_2)_2^-$⊂MOF(Cu) crystals contain $[N(NO_2)_2]^-$ anions. In addition, the mass peak of NO_3^- (m/z = 62) has not been observed in the spectrum, which confirms that NO_3^- in the framework channel has been fully exchanged by $N(NO_2)_2^-$.

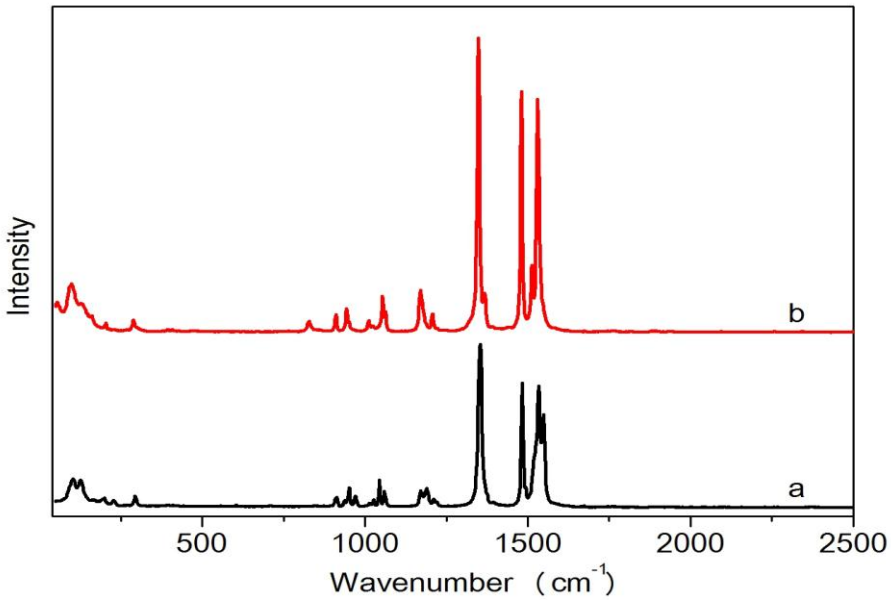

Figure S7. Raman spectra of MOF(Cu) (a) and $N(NO_2)_2^-$ ⊂ MOF(Cu) (b)

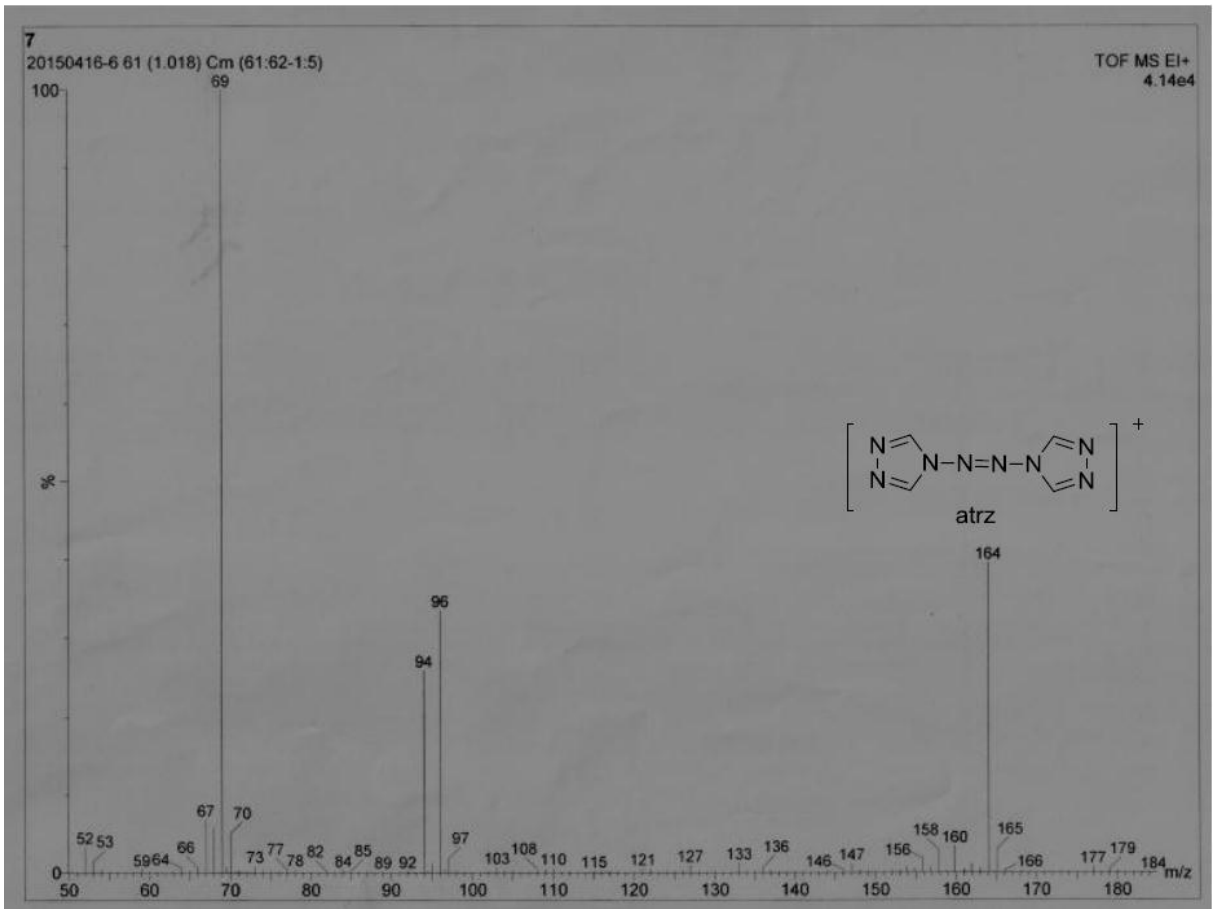

Figure S8. EI spectrum of $N(NO_2)_2^-$⊂MOF(Cu). The result showed that $N(NO_2)_2^-$ ⊂MOF(Cu) contains atrz ligands (M^+, m/z=164).

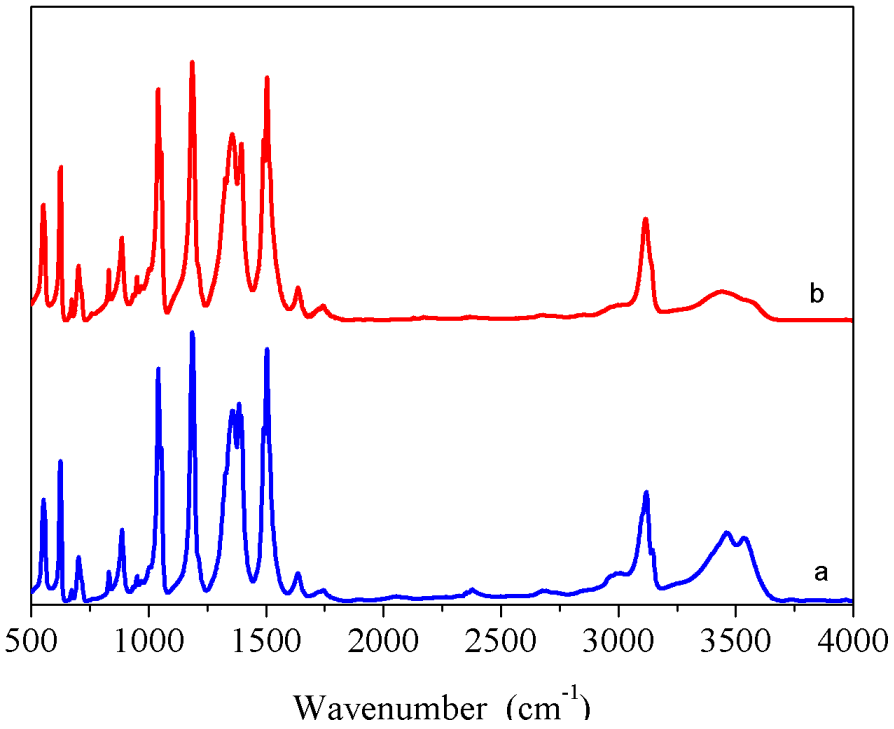

Figure S9. IR spectra of $N(NO_2)_2^-$⊂MOF(Cu): a) as-prepared $N(NO_2)_2^-$⊂MOF(Cu); b) as-prepared $N(NO_2)_2^-$⊂MOF(Cu) after desolvated.

The IR spectrum of $N(NO_2)_2^-$⊂MOF(Cu) is almost identical with that of $N(NO_2)_2^-$⊂MOF(Cu) after desolvated from 500 to 3250 cm^{-1}, which shows that the framework remains intact after the remove of guest water molecules. The band of water (3500 cm^{-1}) in the IR spectrum of desolvated $N(NO_2)_2^-$⊂MOF(Cu) remarkably decreases in comparison with that in the IR spectrum of $N(NO_2)_2^-$⊂MOF(Cu). It is possible that the guest water molecules were removed during the dehydration process. There is still a weak band (3500 cm^{-1}) in the IR spectrum maybe due to KBr which is not fully dried.

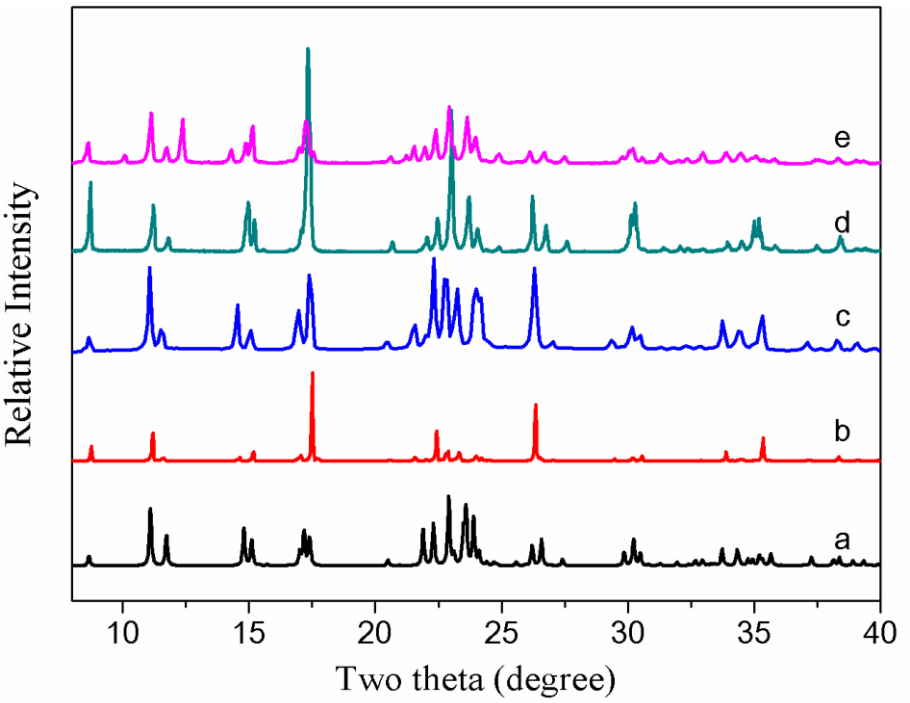

Figure S10. PXRD patterns of various samples: a) the simulated single-crystal diffraction data of $N(NO_2)_2^-$⊂MOF(Cu); b) as-prepared $N(NO_2)_2^-$⊂MOF(Cu); c) $N(NO_2)_2^-$⊂MOF(Cu) after heated at 150 °C for 24 h; d) as-prepared $N(NO_2)_2^-$⊂MOF(Cu) after desolvated; e) as-prepared MOF(Cu).

The PXRD pattern of $N(NO_2)_2^-$⊂MOF(Cu) is almost identical with that of MOF(Cu), suggesting that the framework remains intact throughout the anion exchange process. In addition, the PXRD patterns indicated that $N(NO_2)_2^-$⊂MOF(Cu) is also intact even after it has been heated at 150 °C for 24 h in air.

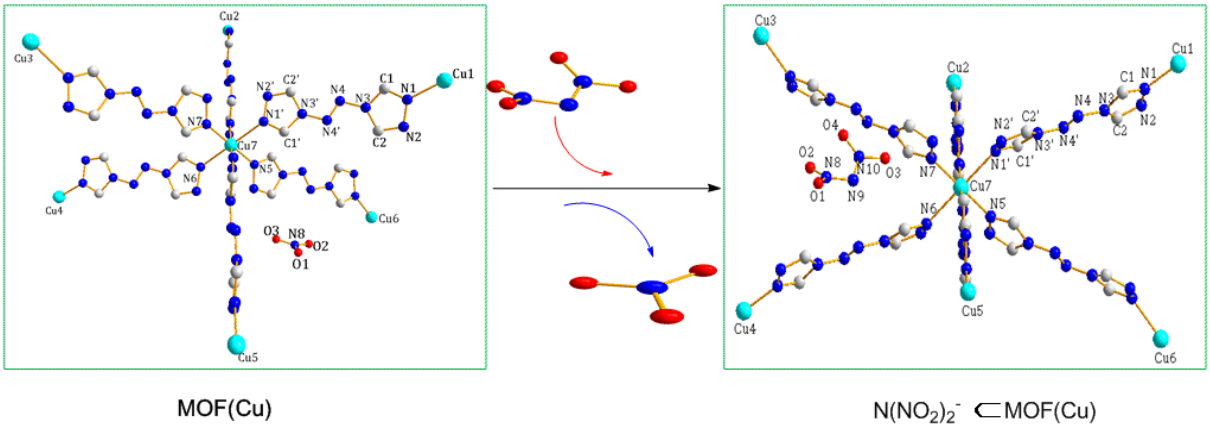

Figure S11. (Left) Coordination structure of MOF(Cu). (Right) Coordination structure of $N(NO_2)_2^- \subset$MOF(Cu). In the molecular structure of $N(NO_2)_2^- \subset$MOF(Cu), the Cu^{II} atom is six-coordinated by six atrz nitrogen atoms in a regular octahedron, which is consistent with that of the Cu^{II} atom in the structure of MOF(Cu). Hydrogen atoms, guest water and more anions have been omitted for clarity.

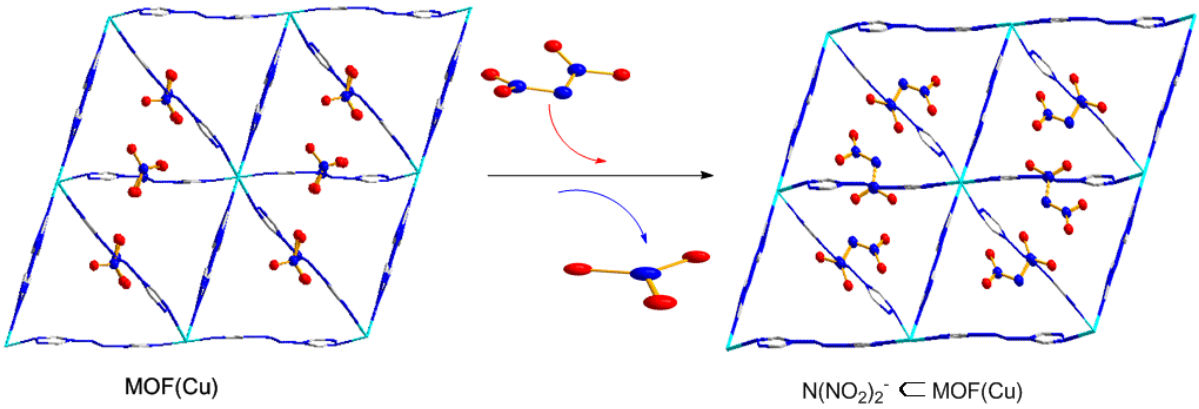

Figure S12. (Left) The crystal packing of MOF(Cu) viewed along the crystallographic a axis. (Right) The crystal packing of $N(NO_2)_2^- \subset$MOF(Cu) viewed along the crystallographic a axis. The scheme is shown for the exchange process of trapping $N(NO_2)_2^-$ anions and loss of NO_3^- anions. Hydrogen atoms and guest water have been omitted for clarity.

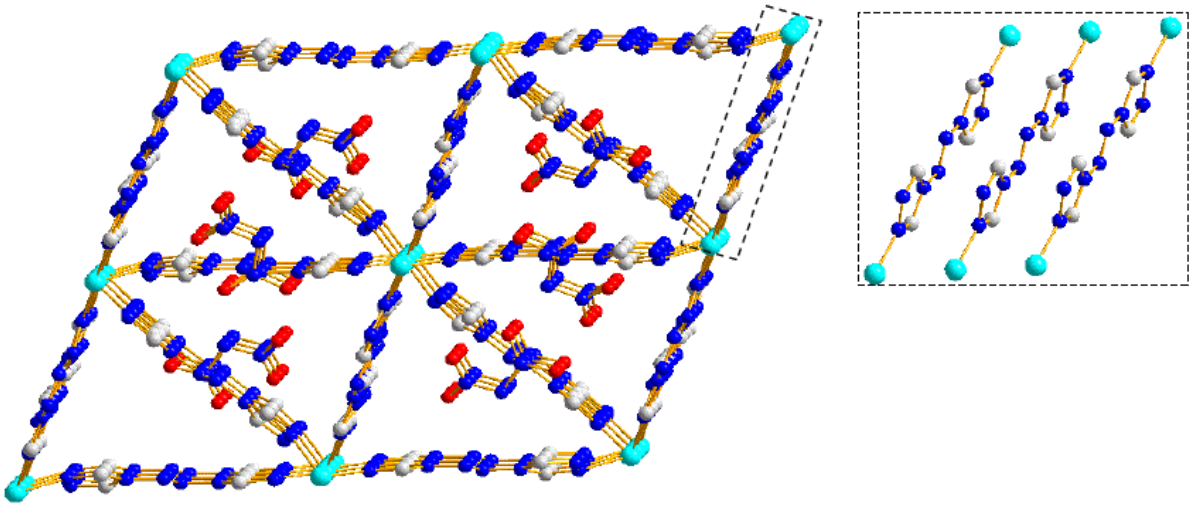

Figure S13. Packing structure of $N(NO_2)_2^-$⊂MOF(Cu) highlighting the coordination mode of atrz

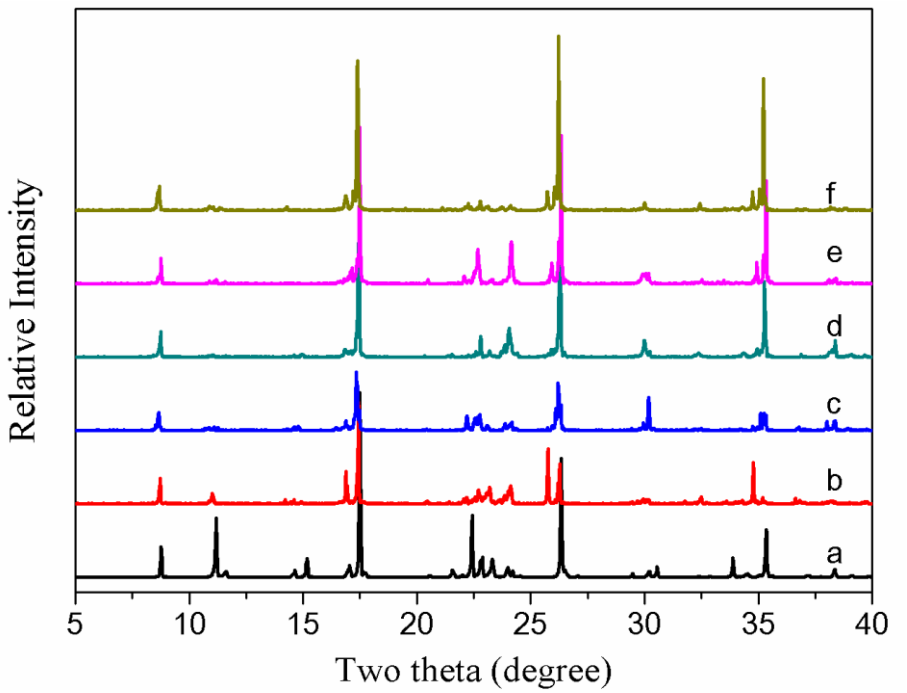

Figure S14. PXRD patterns of as-prepared $N(NO_2)_2^-$ ⊂ MOF(Cu) in various HNO_3/NaOH aqueous solutions with different pH values for 24 hours: a) as-prepared $N(NO_2)_2^-$⊂MOF(Cu); b) pH=1; c) pH=4; d) pH=7; e) pH=10; f) pH=14. The PXRD patterns showed that $N(NO_2)_2^-$⊂MOF(Cu) can keep its crystallinity after immersion in HNO3/NaOH aqueous solutions with pH values ranging from 0 to 10 for 24 h.

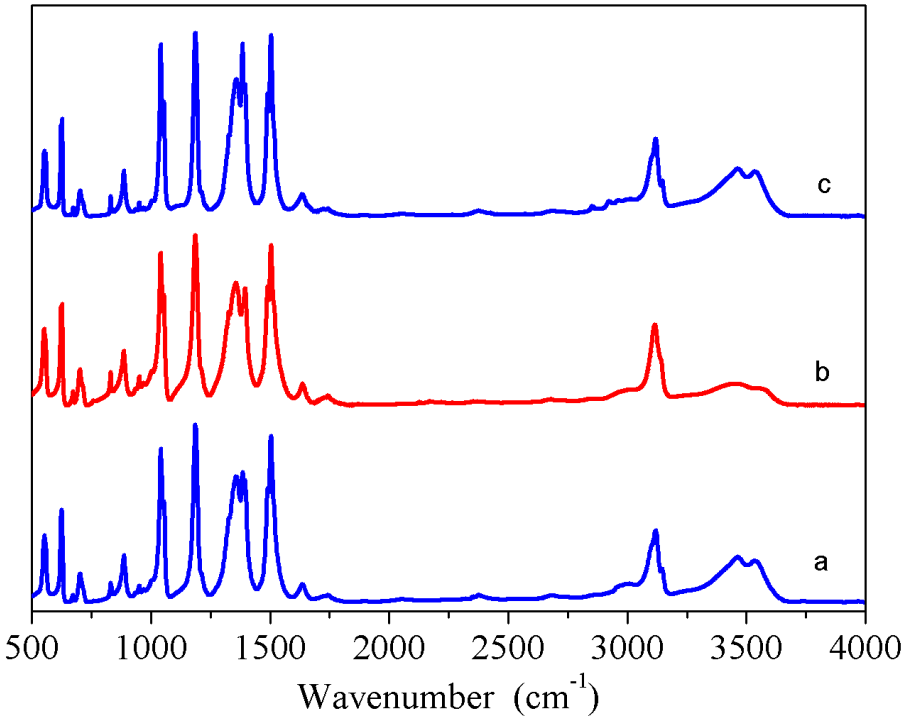

Figure S15. IR spectra of various samples : a) as-prepared $N(NO_2)_2^- \subset$MOF(Cu); b) $N(NO_2)_2^- \subset$MOF(Cu) after heated at 150 °C for 24 h; c) as-prepared MOF(Cu).

The IR spectrum of $N(NO_2)_2^- \subset$MOF(Cu) is almost identical with that of MOF (Cu), which shows that the framework remains intact throughout the anion exchange process. In addition, the above spectra showed $N(NO_2)_2^- \subset$MOF(Cu) remains intact after heated at 150 °C for 24 h.

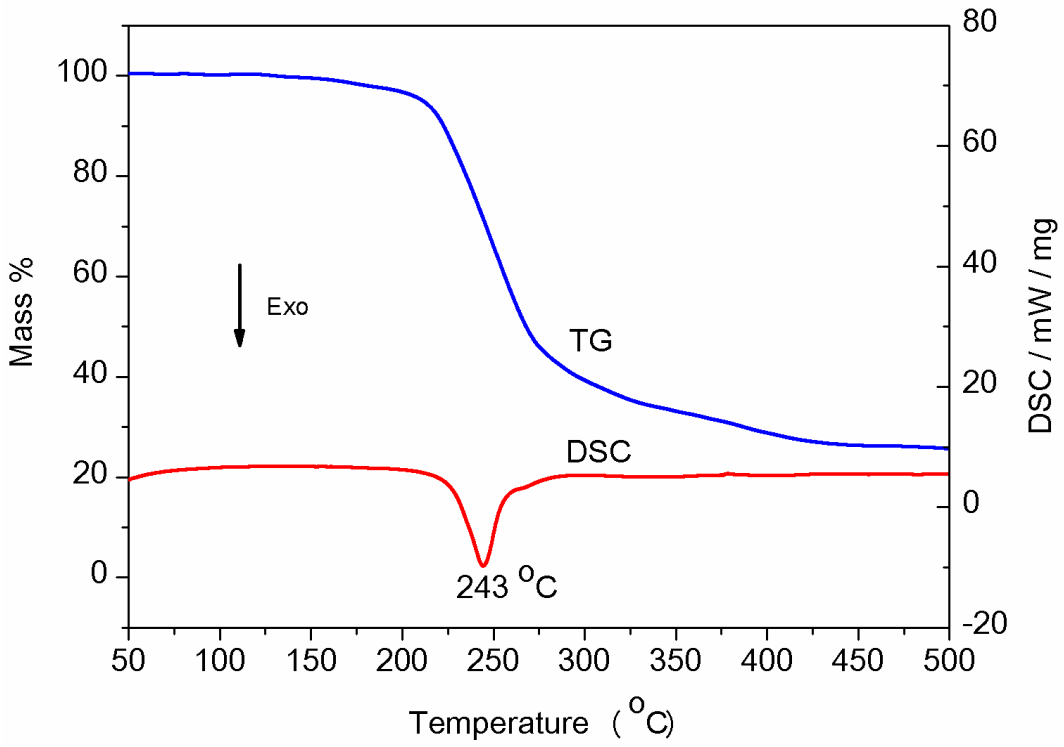

Figure S16. TG/DSC curves of as-synthesized $N(NO_2)_2^- \subset$MOF(Cu)

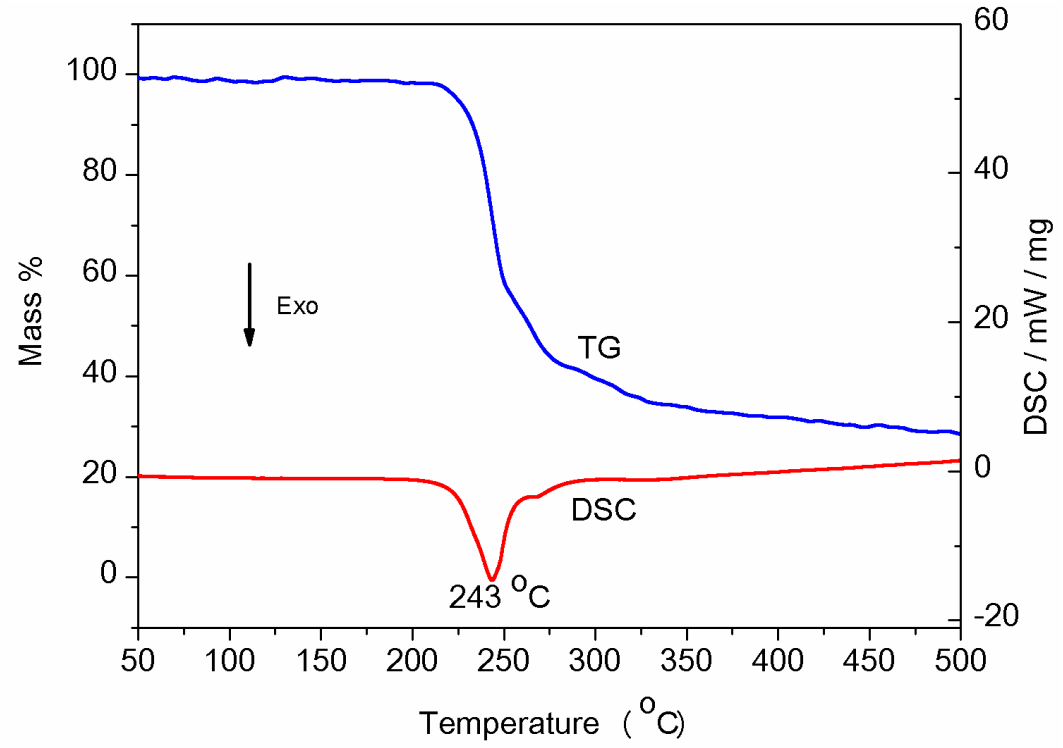

Figure S17. TG/DSC curves of dehydrated $N(NO_2)_2^- \subset$MOF(Cu). The results showed that the onset decomposition temperature (221 °C) of dehydrated $N(NO_2)_2^- \subset$MOF(Cu) is consistent with that of as-synthesized $N(NO_2)_2^- \subset$MOF(Cu). Since the PXRD patterns and IR spectra (**Figure S10 and S15**) indicated that $N(NO_2)_2^- \subset$MOF(Cu) is intact even after it has been heated at 150 °C for 24 h in air, the dehydrated sample is also intact.

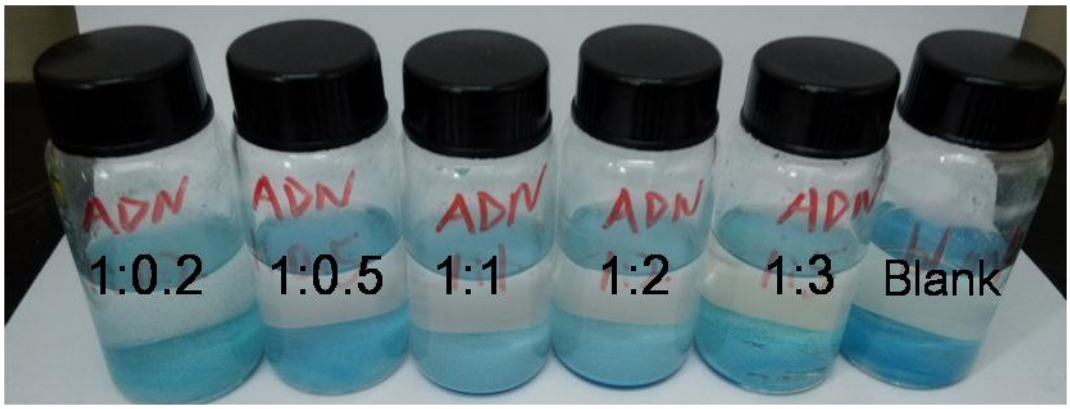

Figure S18. Photographs of MOF(Cu) powders after immersion in various concentrations of ADN solutions after 7 days at room temperature. The mole ratios of AND to MOF(Cu) were 0.2:1, 0.5:1, 1:1, 2:1, and 3:1, and 1:0 (blank).

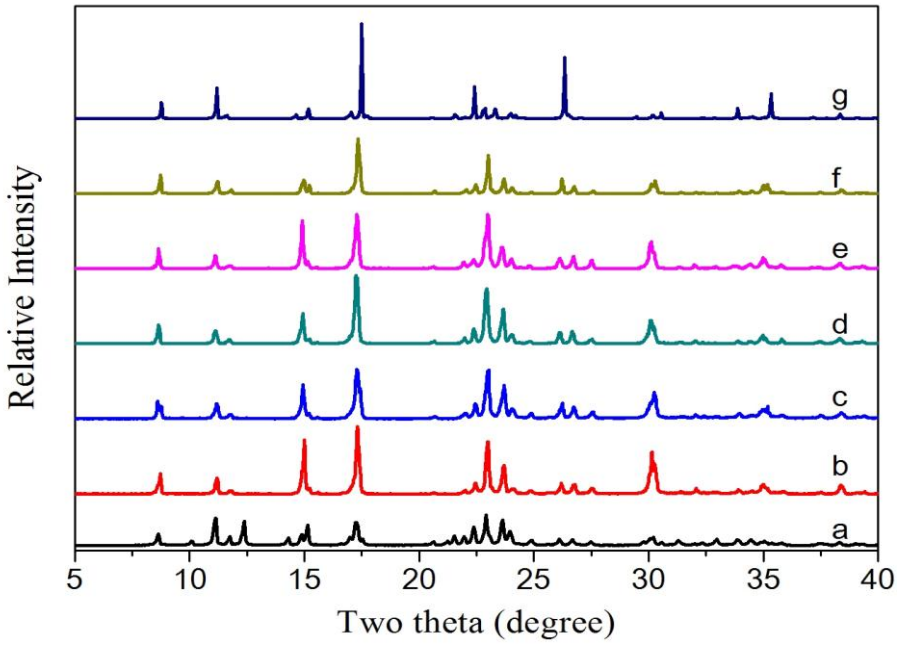

Figure S19. PXRD patterns of as-prepared MOF(Cu) (a), as-prepared $N(NO_2)_2^-$ ⊂MOF(Cu) (g) and various products after anion exchange between ADN and MOF(Cu) at different mole ratios: b) 0.2:1; c) 0.5:1; d) 1:1; e) 2:1; f) 3:1.

The PXRD patterns of various products were almost identical with that of MOF(Cu), suggesting that the framework remained intact throughout the anion exchange process.

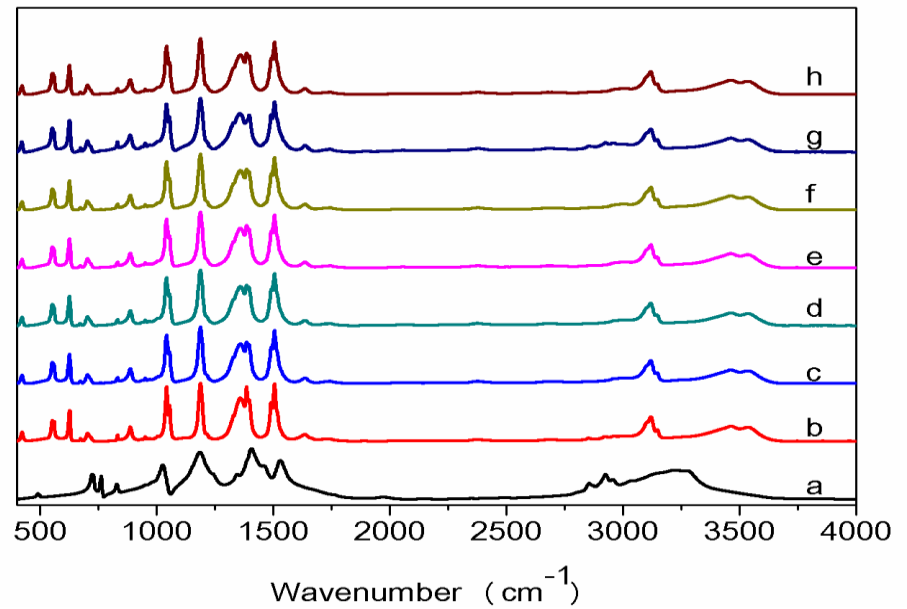

Figure S20. IR spectra of ADN(a), as-prepared MOF(Cu) (b) and various products after anion exchange between AND and MOF(Cu) at different mole ratios: c) 0.2:1; d) 0.5:1; e) 1:1; f) 2:1; g) 3:1; h) as-prepared $N(NO_2)_2^- \subset$MOF(Cu) crystals.

The IR spectra of various products were almost identical with that of MOF(Cu), suggesting that the framework remained intact throughout the anion exchange process.

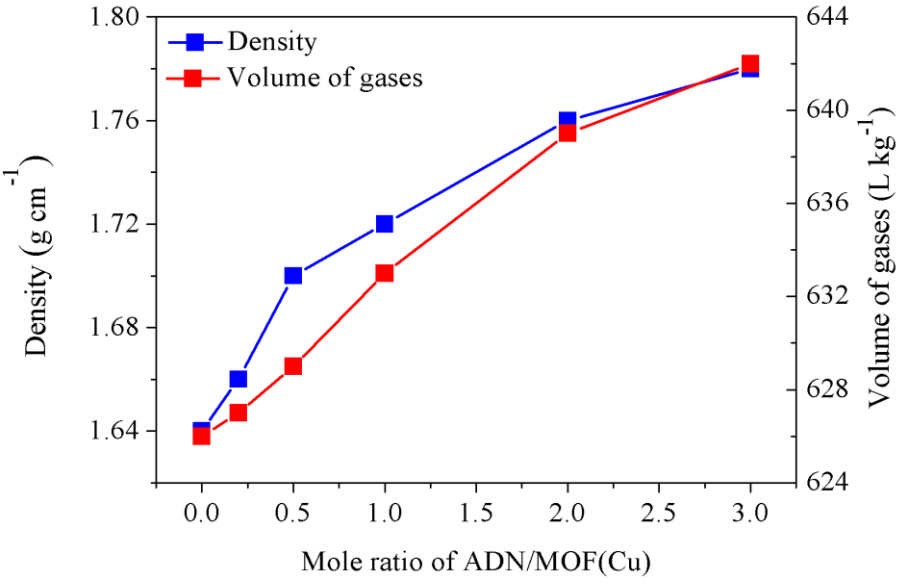

Figure S21. Tunable densities and volume of gases after detonation of the resultant complexes through changing the mole ratio of ADN/MOF(Cu) in the reaction mixture

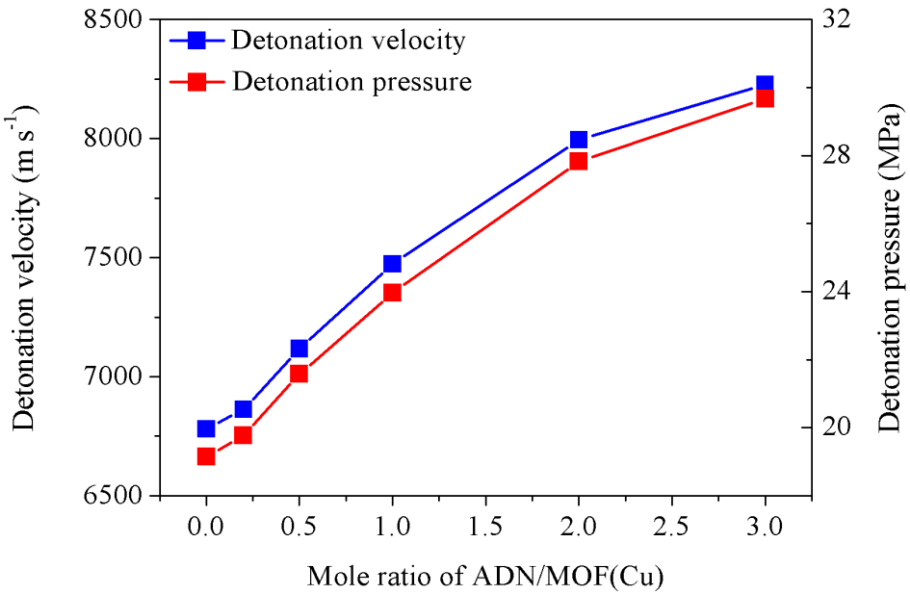

Figure S22. Tunable detonation velocities and pressures of the resultant complexes through changing the mole ratio of ADN/MOF(Cu) in the reaction mixture

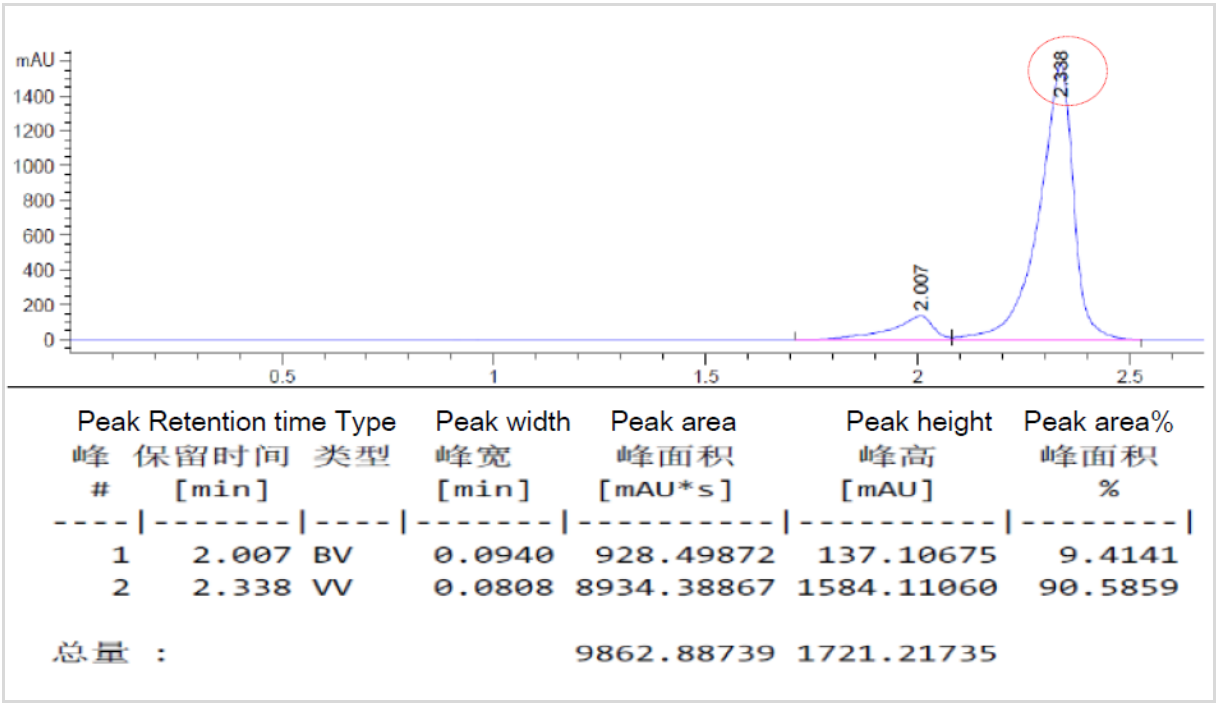

Peak #	Retention time [min]	Type	Peak width [min]	Peak area [mAU*s]	Peak height [mAU]	Peak area %
1	2.007	BV	0.0940	928.49872	137.10675	9.4141
2	2.338	VV	0.0808	8934.38867	1584.11060	90.5859
总量 :				9862.88739	1721.21735	

Figure S23. HPLC spectrum of 6.2 mg ADN in 10 ml water (5 mmol L^{-1}, retention time: 2.338 min; peak area: 8934.39, eluent: 10% CH_3OH in water; flow rate: 1 mL min^{-1}).

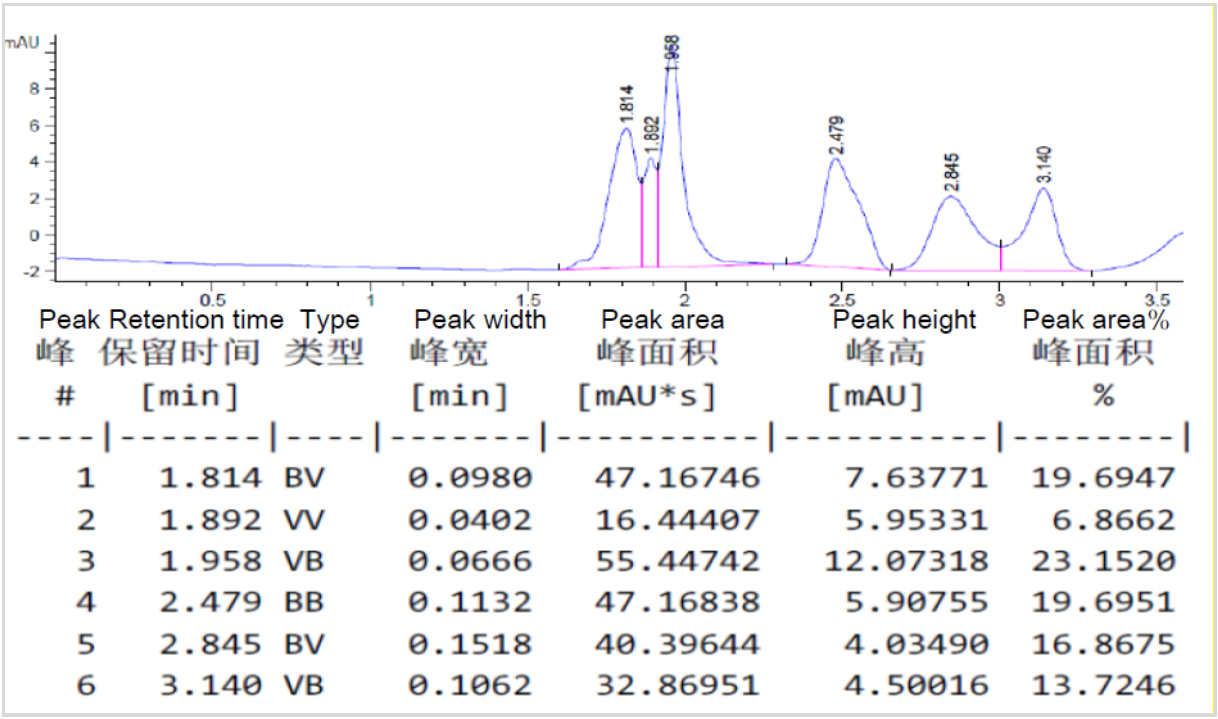

Peak 峰 #	Retention time 保留时间 [min]	Type 类型	Peak width 峰宽 [min]	Peak area 峰面积 [mAU*s]	Peak height 峰高 [mAU]	Peak area% 峰面积 %
1	1.814	BV	0.0980	47.16746	7.63771	19.6947
2	1.892	VV	0.0402	16.44407	5.95331	6.8662
3	1.958	VB	0.0666	55.44742	12.07318	23.1520
4	2.479	BB	0.1132	47.16838	5.90755	19.6951
5	2.845	BV	0.1518	40.39644	4.03490	16.8675
6	3.140	VB	0.1062	32.86951	4.50016	13.7246

Figure S24. HPLC spectrum of 0.16 g $N(NO_2)_2^-$⊂MOF(Cu) crystals in 10 ml water (eluent: 10% CH_3OH in water; flow rate: 1 mL min^{-1}).

The HPLC result showed that all peak heights are extremely low(<13 mAU) and all peak area are very small (<56 mAU.s) , while 5 mmol L^{-1} ADN corresponds to 8934.39 mAu.s peak area at the same HPLC condition (Figure S23). Therefore, $N(NO_2)_2^-$⊂MOF(Cu) crystals is almost insoluble in water.

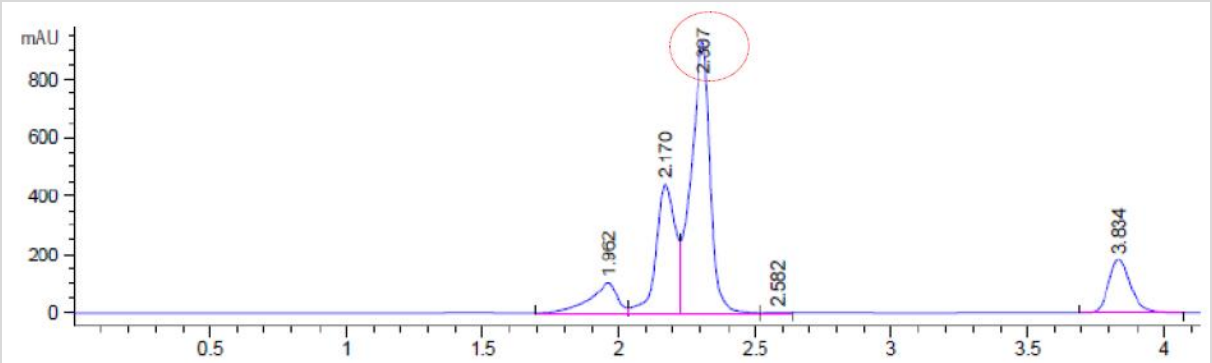

Peak # 峰	Retention time 保留时间 [min]	Type 类型	Peak width 峰宽 [min]	Peak area 峰面积 [mAU*s]	Peak height 峰高 [mAU]	Peak area% 峰面积 %
1	1.962	BV	0.0943	705.54962	103.84335	8.3439
2	2.170	VV	0.0760	2207.67358	443.76788	26.1081
3	2.307	VB	0.0709	4539.33301	931.31042	53.6824
4	2.582	BV	0.0769	9.03962	1.73150	0.1069
5	3.834	VV	0.0839	994.31006	181.43768	11.7588
总量 :				8455.90590	1662.09083	

Figure S25. HPLC spectrum of the reaction solution after anion release between $N(NO_2)_2^-$⊂MOF(Cu) and NaN_3 [the mole ratio of NaN3 and $N(NO_2)_2^-$⊂MOF(Cu) is 2:1].

0.16 g $N(NO_2)_2^-$⊂MOF(Cu) (0.2 mmol) was immersed in a 10 mL aqueous solution of NaN_3 (0.04 mol/L). After anion release, the resultant crystals were filtrated and washed thoroughly with deionized water. The filtration solution was further diluted with water to 15 ml. The diluted sample was determined by HPLC-MS (eluent: 10 % CH_3OH in water; flow rate: 1 mL min^{-1}). The retention time of $N(NO_2)_2^-$ is 2.307 min, its peak area is 4539.33 mAU.s, while 5 mmol L^{-1} ADN corresponds to 8934.39 mAu.s peak area at the same HPLC condition. The concertration of $N(NO_2)_2^-$ in the reaction solution after anion release is about 3.81 mol/L. The released $N(NO_2)_2^-$ content from $N(NO_2)_2^-$⊂MOF(Cu) is 95.3% (3.81/0.4). Therefore, the HPLC result showed that the encapsulated $N(NO_2)_2^-$ in the framework of $N(NO_2)_2^-$⊂MOF(Cu) was almost completely released into the reaction solution.

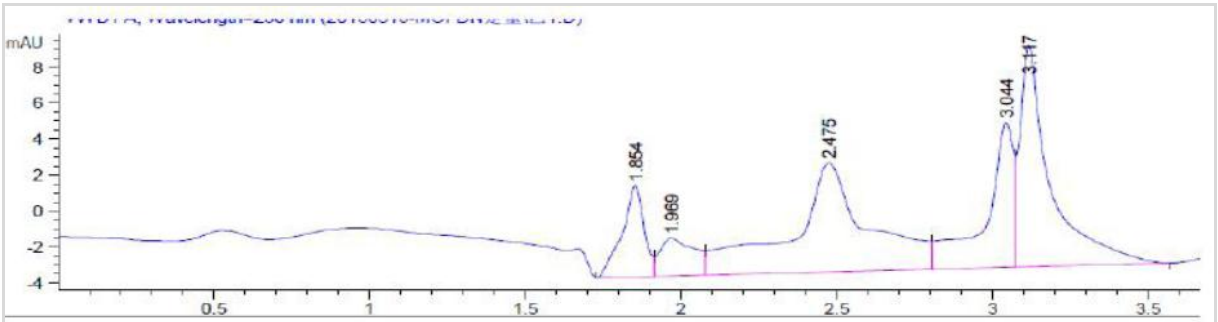

Peak # 峰	Retention time [min] 保留时间	Type 类型	Peak width [min] 峰宽	Peak area [mAU*s] 峰面积	Peak height [mAU] 峰高	Peak area % 峰面积
1	1.854	BV	0.0695	25.07030	5.08235	8.9709
2	1.969	VV	0.1042	16.10163	2.10481	5.7616
3	2.475	VV	0.2266	104.08803	6.08269	37.2456
4	3.044	VV	0.0868	51.07341	8.07723	18.2755
5	3.117	VB	0.0909	83.13046	12.28800	29.7464

Figure S26. HPLC spectrum of 0.16 g $N(NO_2)_2^-$⊂MOF(Cu) crystals in 10 mL methanol (eluent: 10% CH_3OH in water; flow rate: 1 mL min^{-1}).

The HPLC result showed that all peak heights are extremely low(<13 mAU) and all peak areas are very small (<105 mAU.s) , while 5 mmol L^{-1} ADN corresponds to 8934.39 mAu.s peak area at the same HPLC condition (Figure S23). Therefore, the $N(NO_2)_2^-$⊂MOF(Cu) crystal is almost insoluble in methanol.

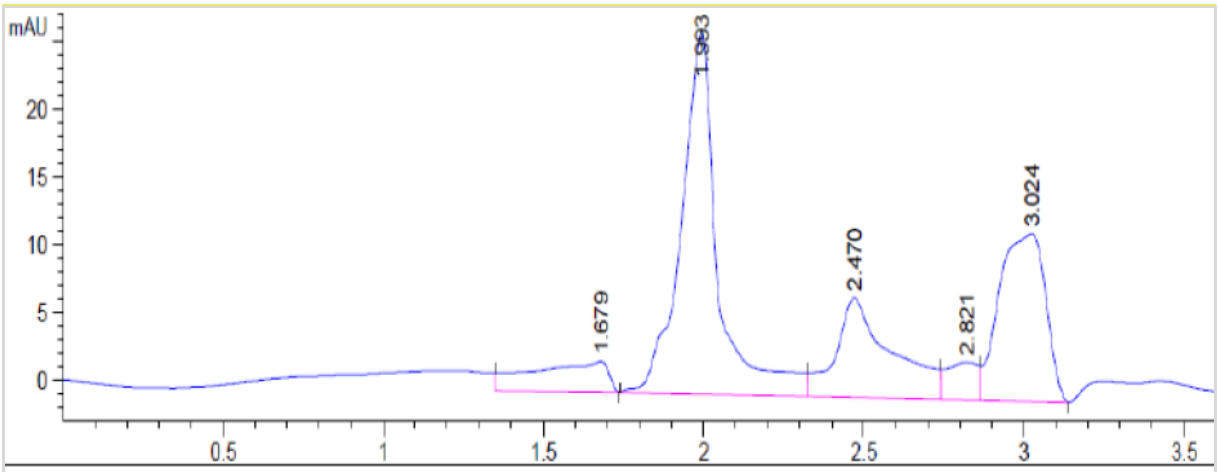

Peak 峰 #	Retention time 保留时间 [min]	Type 类型	Peak width 峰宽 [min]	Peak area 峰面积 [mAU*s]	Peak height 峰高 [mAU]	Peak area% 峰面积 %
1	1.679	VB	0.2046	37.14404	2.27351	7.7130
2	1.993	BV	0.1128	212.37309	26.70066	44.0992
3	2.470	VV	0.1617	89.20091	7.34285	18.5226
4	2.821	VV	0.0997	18.90186	2.76664	3.9250
5	3.024	VB	0.1359	123.95993	12.37574	25.7403

Figure S27. HPLC spectrum of 0.16 g $N(NO_2)_2^-$⊂MOF(Cu) crystals in 10 mL acetonitrile (eluent: 10% CH_3OH in water; flow rate: 1 mL min^{-1}).

The HPLC result showed that all peak heights are extremely low(<27 mAU) and all peak areas are very small (<213 mAU.s) , while 5 mmol L^{-1} ADN corresponds to 8934.39 mAu.s peak area at the same HPLC condition (Figure S23). Therefore, the $N(NO_2)_2^-$⊂MOF(Cu) crystal is almost insoluble in acetonitrile.

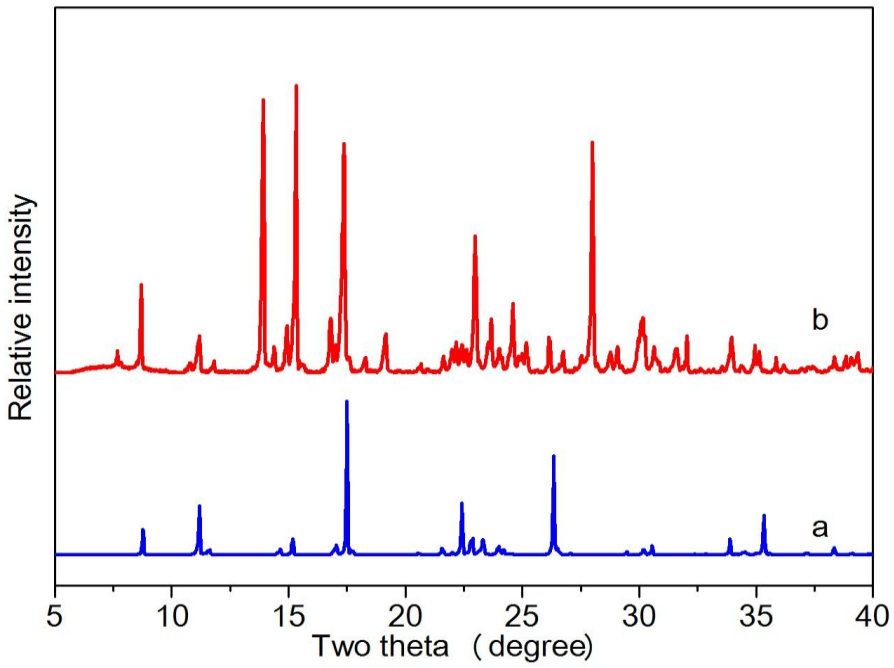

Figure S28. PXRD patterns of $N(NO_2)_2^- \subset$MOF(Cu) (a) and $N_3^- \subset$MOF(Cu) (b). The PXRD patterns showed many main peaks of $N_3^- \subset$MOF(Cu) are almost identical with that of $N(NO_2)_2^- \subset$ MOF(Cu), suggesting that the framework remains intact throughout the release process.

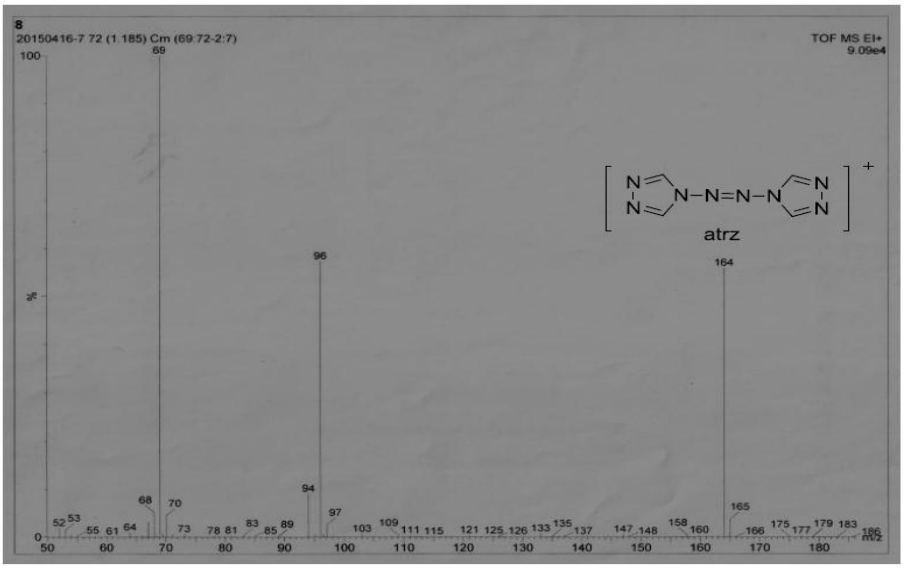

Figure S29. EI spectrum of $N_3^- \subset$MOF(Cu). The result showed that $N_3^- \subset$MOF(Cu) contains atrz ligands (M=164)

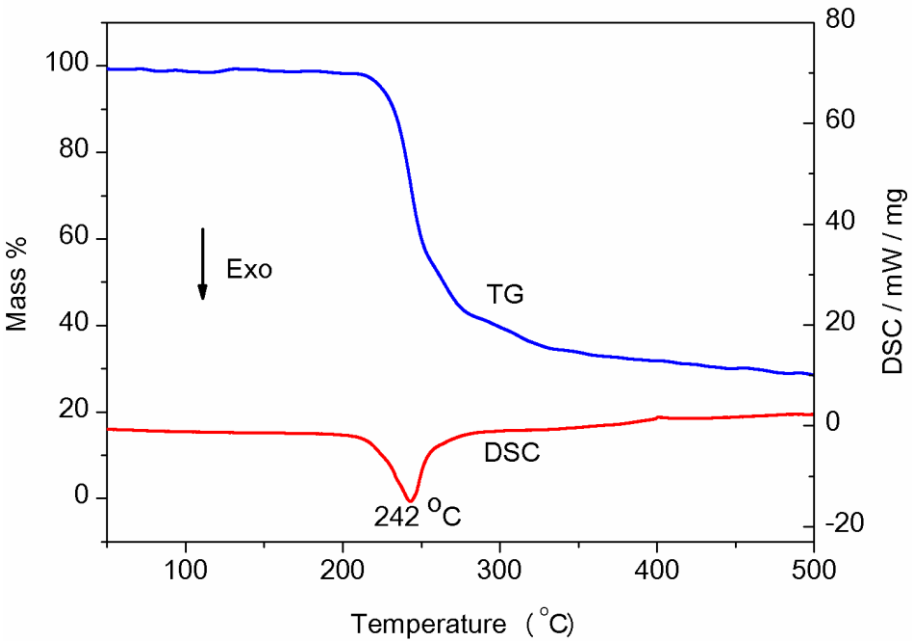

Figure S30. DSC curve of $N_3^- \subset$MOF(Cu)

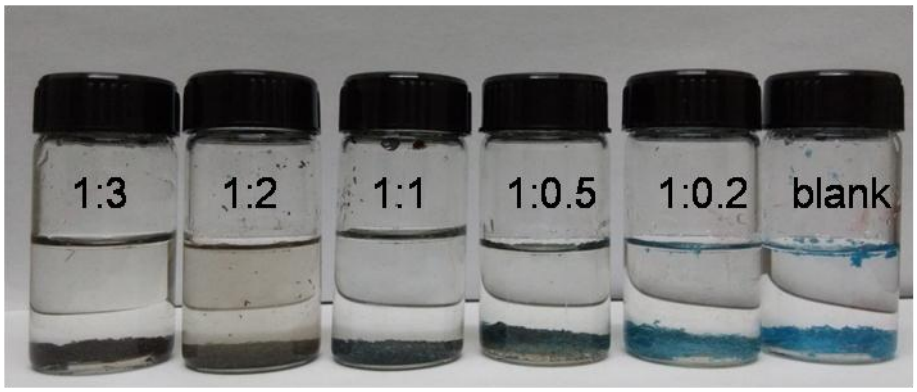

Figure S31. Photograph of $N(NO_2)_2^- \subset$ MOF(Cu) after immersion in various concentration of NaN_3 solutions after 30 min at room temperature. The molar ratios of NaN_3 to $N(NO_2)_2^- \subset$MOF(Cu) are 0.2:1, 0.5:1, 1:1, 2:1, and 3:1, respectively.

During the release process of $N(NO_2)_2^-$, the crystals of $N(NO_2)_2^- \subset$MOF(Cu) underwent a rapid naked-eye detectable change in color(from blue to deep brown); the concomitant solid products were in the bottom of the vial, which can be obtained through simple filtration. As the mole ratio of $NaN_3/N(NO_2)_2^- \subset$MOF(Cu) increased, the color of solid product became more and more deep.

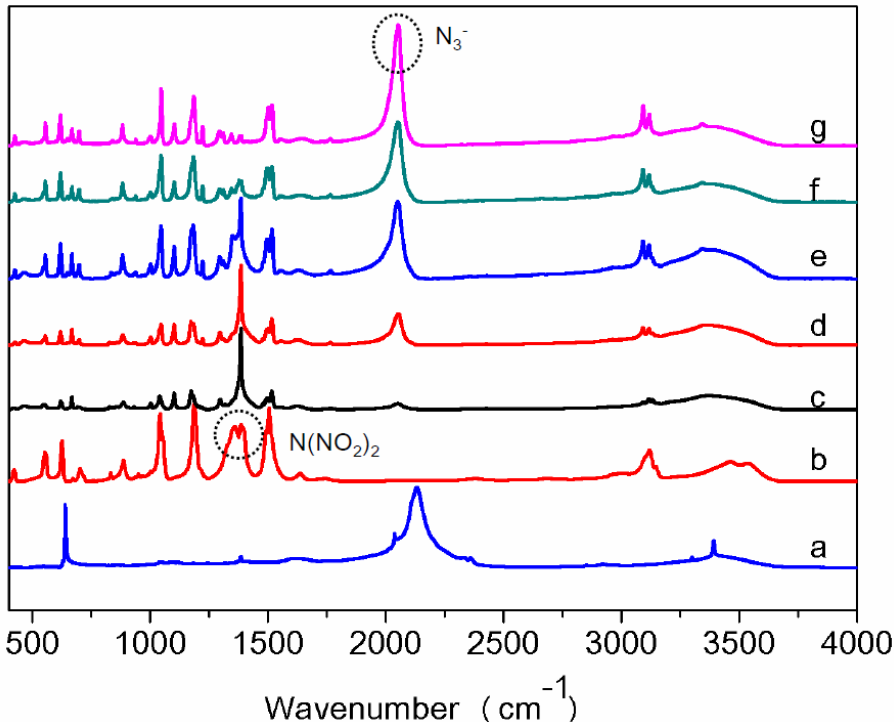

Figure S32. IR spectra of NaN_3 (a), $N(NO_2)_2^- \subset$MOF(Cu) (b) and various solid products after anion release between NaN_3 and $N(NO_2)_2^- \subset$MOF(Cu) at different mole ratio: c) 0.2:1; d) 0.5:1; e) 1:1; f) 2:1; g) 3:1.

As the mole ratio of NaN_3 and $N(NO_2)_2^- \subset$MOF(Cu) increases, the band associated with the encapsulated anion N_3^- (2050 cm^{-1}) becomes stronger and stronger while the band of $N(NO_2)_2^-$ (1390 cm^{-1}) becomes lower and lower.

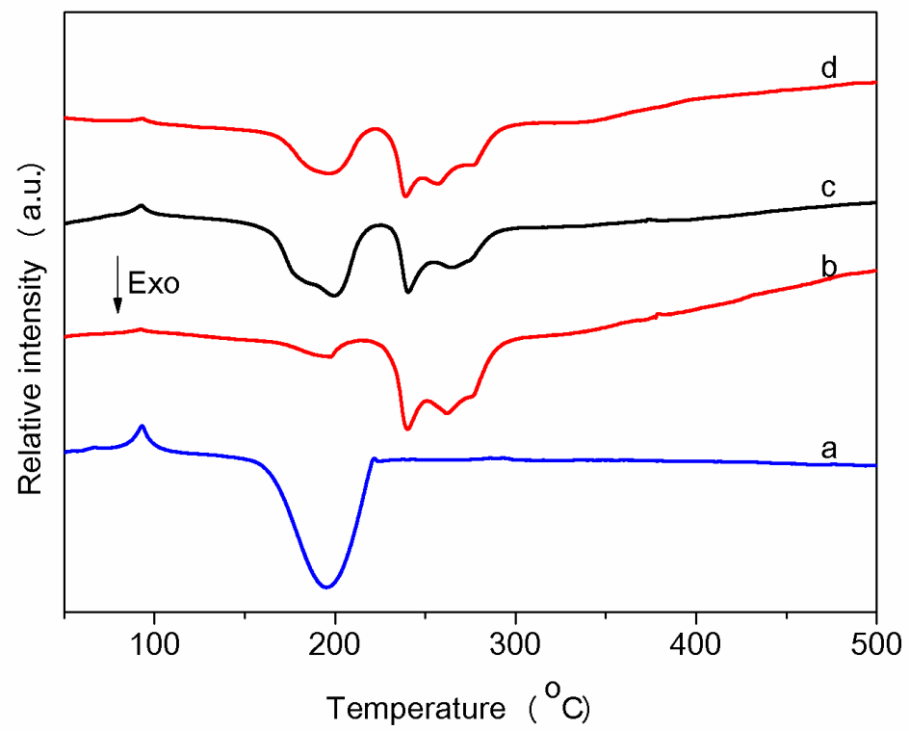

Figure S33. DSC curves of ADN (a) and the mixtures of ADN and MOF(Cu) at various molar ratios under physical mixing. The mole ratios of ADN and MOF(Cu) were 2:1 (b), 1:1 (c), and 0.5:1 (d), respectively.

DSC curves showed that the thermal stability of ADN has not obviously been improved through physically mixing with MOF(Cu) since their onset decomposition temperatures are still identical.

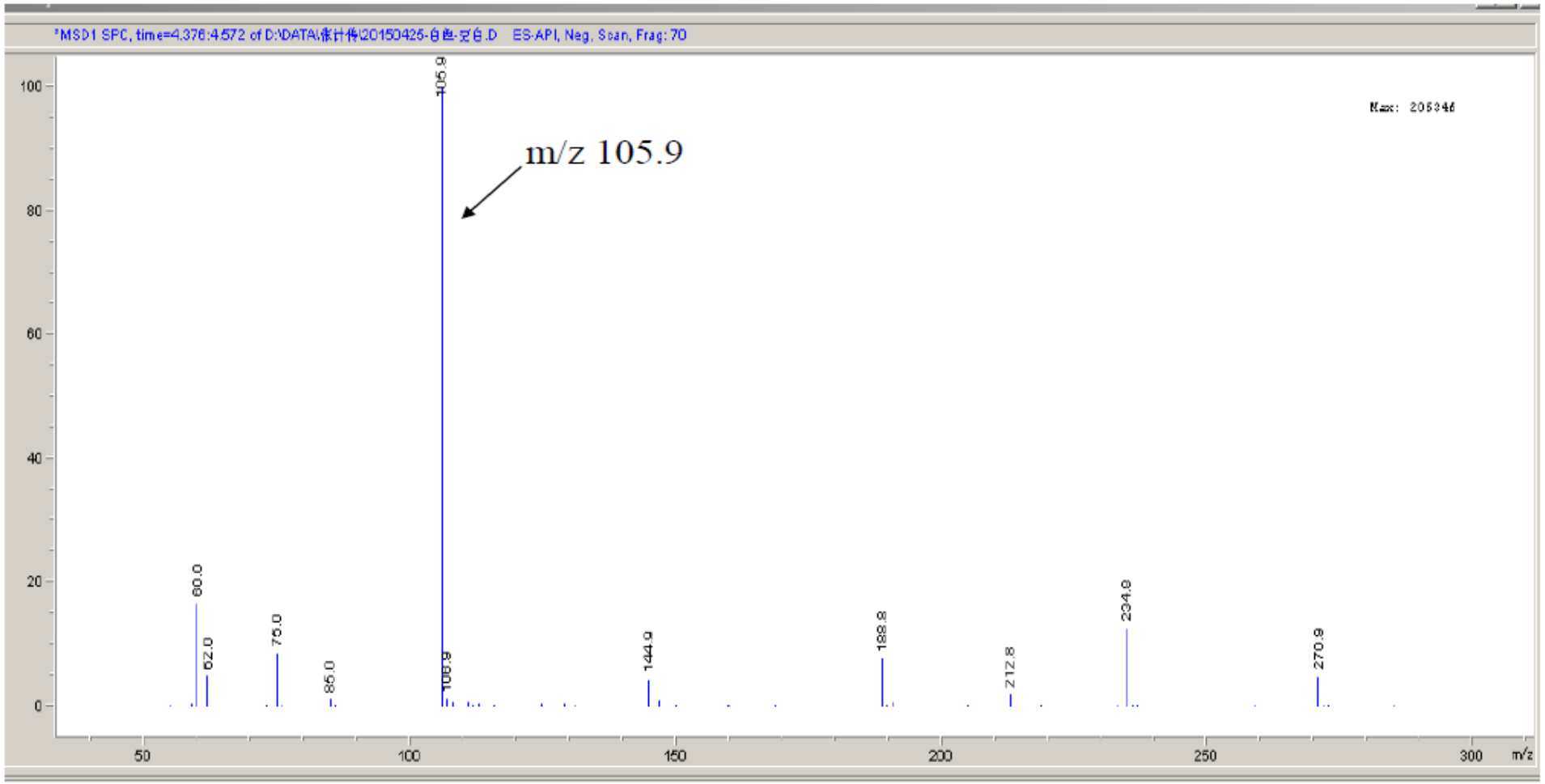

Figure S34. ESI-MS spectrum of the reaction solution after the release of $N(NO_2)_2^-$ from $N(NO_2)_2^-\subset$MOF(Cu). The molar ratio of NaN_3 to $N(NO_2)_2^-\subset$MOF(Cu) is 2:1. ($N(NO_2)_2^-$): $[M]^+$, m/z=105.9. According to ESI-MS analysis, the release of $N(NO_2)_2^-$ from the framework into the aqueous solution was evidenced by the appearance of a mass peak at 106 m/z (M^+).

REFERENCE

(1) Li, S.; Wang, Y.; Qi, C.; Zhao, X.; Zhang, J.; Zhang, S.; Ping, S. 3D Energetic Metal–Organic Frameworks: Synthesis and Properties of High Energy Materials. *Angew. Chem. Int. Ed*. **2013**, *52*, 14031-14035.

(2) Lide, D. R. Standard Thermodynamic Properties of Chemical Substances. *CRC Handbook of Chemistry and Physics, Internet Version* **2007**, 87th ed.; Taylor and Francis: Boca Raton, FL, **2007**.

(3) Kamlet, M. J.; Jacobs, S. J. The Chemistry of Detonations. 1. A Simple method for Calculating Detonation Properties of CHNO Explosives. *J. Chem. Phys*. **1968**, *48*, 23-35.

(4) Wang, Y.; Zhang, J.; Su, H.; Li, S.; Zhang, S.; Pang, S. A Simple Method for the Prediction of the Detonation Performances of Metal-Containing Explosives. *J. Phys. Chem. A*. **2014**, 118, 4575-4581.

(5) Klapötke, T. M.; Schmid, P. C.; Schnell, S.; Stierstorfer, J. 3,6,7-Triamino-[1,2,4] triazolo[4,3-b][1,2,4]triazole: A Non-Toxic, High-Performance Energetic Building Block with Excellent Stability. *Chem. Eur. J*. **2015**, *21*, 9219-9228.

(6) Fischer, D.; Klapötke, T. M.; Stierstorfer, J. 1,5-Di (nitramino) tetrazole: High Sensitivity and Superior Explosive Performance. *Angew. Chem. Int. Ed*. **2015**, *54*, 10299-10302.

(7) Christe, K. O.; Wilson, W. W.; Petrie, M. A.; Michels, H. H.; Bottaro, J. C.; Gilardi, R. The Dinitramide Anion, $N(NO_2)_2^-$. *Inorganic Chemistry*, **1996**, *35*, 5068-5071.

(8) Gilardi, R.; Flippen-Anderson, J.; George, C.; Butcher, R. J. A New Class of Flexible Energetic Salts: The Crystal Structures of the Ammonium, Lithium, Potassium, and Cesium Salts of Dinitramide. *J. Am. Chem. Soc*. **1997**, *119*, 9411-9416.

(9) Ang, H. -G.; Fraenk, W.; Karaghiosoff, K.; Klapötke, T. M.; Mayer, P.; Nöth, H.; Sprott, J.; Warchhold, M. Synthesis, Characterization, and Crystal Structures of Cu, Ag, and Pd Dinitramide Salts, *Z. Anorg. Allg. Chem*. **2002**, *628*, 2894-2900.

(10) Klapötke, T. M.; Schmid, P.; Schnell, S.; Stierstorfer, J. Thermal Stabilization of Energetic Materials by the Aromatic Nitrogen-Rich 4,4′-5,5′-Tetraamino-3,3′-Bi-1,2,4-Triazolium Cation, *J. Mater. Chem. A*, 2015, *3*, 2658-2668.

(11) Klapötke, T. M.; Stierstorfer, J. The New Energetic Compounds 1,5-Diaminotetrazolium and 5-Amino-1-methyltetrazolium Dinitramide-Synthesis, Characterization and Testing. *Eur. J. Inorg. Chem.* **2008**, 4055–4062.

(12) Klapötke, T. M.; Stierstorfer, J. Azidoformamidinium and 5-Aminotetrazolium Dinitramide-Two Highly Energetic Isomers with a Balanced Oxygen Content. *Dalton Trans.*, **2009**, 643–653.

(13) Yin, P.; Parrish, D. A.; Shreeve, J. M. Energetic Multifunctionalized Nitraminopyrazoles and Their Ionic Derivatives: Ternary Hydrogen-Bond Induced High Energy Density Materials. *J. Am. Chem. Soc.* **2015**, *137,* 4778-4786.

(14) Dippold, A. A.; Klapötke, T. M. A Study of Dinitro-Bis-1,2,4-Triazole-1,1′-Diol and Derivatives: Design of High-Performance Insensitive Energetic Materials by the Introduction of N-Oxides. *J. Am. Chem. Soc.* **2013**, *135,* 9931-9938.

(15) He, C.; Shreeve, J. M. Energetic Materials with Promising Properties: Synthesis and Characterization of 4,4′-Bis(5-Nitro-1,2,3-2H-Triazole) Derivatives. *Angew. Chem. Int. Ed.* **2015**, *54*, 6260-6264.

(16) Wei, H.; He, C.; Zhang, J.; Shreeve, J. M. Combination of 1,2,4-Oxadiazole and 1,2,5-Oxadiazole Moieties for the Generation of High-Performance Energetic Materials. *Angew. Chem. Int. Ed.* **2015**, *54*, 9367-9371.

(17) Fischer, D.; Klapötke, T. M. 1,5-Di(nitramino)Tetrazole: High Sensitivity and Superior Explosive Performance. *Angew. Chem. Int. Ed.* **2015**, *54*, 10299-10302.

(18) Göbel, M.; Karaghiosoff, K.; Klapötke, T. M.; Piercey, D. G.; Stierstorfer, J. Nitrotetrazolate-2N-Oxides and the Strategy of N-Oxide Introduction. *J. Am. Chem. Soc.* **2010**, *132*, 17216-17226.

(19) Huynh, M. H. V.; Hiskey, M. A.; Hartline, E. L.; Montoya, D. P.; Gilardi, R. Polyazido High-Nitrogen Compounds: Hydrazo- and Azo-1,3,5-Triazine. *Angew. Chem. Int. Ed.* **2004**, *43,* 4924-4928.

(20) Chavez, D. E.; Hiskey, M. A.; Gilardi, R. D. 3,3′-Azobis (6-Amino-1,2,4,5-Tetrazine): A Novel High-Nitrogen Energetic Material. *Angew. Chem. Int. Ed.* **2000,** *39,* 1791-1793.